

# Synaptic plasticity is required for oscillations in a V1 cortical column model with multiple interneuron types

Giulia Moreni<sup>1,2,\*</sup>, Cyriel M. A. Pennartz<sup>1,2</sup> and Jorge F. Mejias<sup>1,2,\*</sup>

<sup>1</sup>Cognitive and Systems Neuroscience Group, Swammerdam Institute for Life Sciences, Faculty of Science, University of Amsterdam, 1090 GE Amsterdam, the Netherlands

<sup>2</sup>Research Priority Area Amsterdam Brain and Cognition, University of Amsterdam

\*Corresponding author: Giulia Moreni ([g.moreni@uva.nl](mailto:g.moreni@uva.nl)), Jorge F. Mejias ([j.f.mejias@uva.nl](mailto:j.f.mejias@uva.nl))

## Abstract

Neural rhythms are ubiquitous in cortical recordings, but it is unclear whether they emerge due to the basic structure of cortical microcircuits, or depend on function. Using detailed electrophysiological and anatomical data of mouse V1, we explored this question by building a spiking network model of a cortical column incorporating pyramidal cells, PV, SST and VIP inhibitory interneurons, and dynamics for AMPA, GABA and NMDA receptors. The resulting model matched *in vivo* cell-type-specific firing rates for spontaneous and stimulus-evoked conditions in mice, although rhythmic activity was absent. Upon introduction of long-term synaptic plasticity, broad-band (15-60 Hz) oscillations emerged, with feedforward/feedback input streams enhancing/suppressing the oscillatory drive, respectively. These plasticity-triggered rhythms relied on all cell types, and specific experience-dependent connectivity patterns were required to generate oscillations. Our results suggest that neural rhythms are not intrinsic properties of cortical circuits, but rather arise from structural changes elicited by learning-related mechanisms.

## Introduction

Cell-specific activity of cortical networks has been increasingly scrutinized experimentally in recent years, but our mechanistic understanding of cortical dynamics is still incomplete. Fast (>15 Hz) cortical oscillatory activity is a paradigmatic example, as it constitutes a widespread phenomenon, the functional relevance of which is still under debate<sup>1–5</sup>. Fast cortical oscillations may emerge in neural circuits due to a wide range of mechanistic origins, including excitatory-inhibitory interactions, delayed recurrent dynamics, and others<sup>1,6</sup>. The particular postsynaptic receptors involved (i.e. AMPA, GABA, NMDA, etc) are likely to influence qualities such as oscillatory frequency<sup>7</sup>. Likewise, neural oscillations have been found to depend not only on simple excitatory-inhibitory interactions<sup>7–9</sup>, but also on interactions between different cell types such as parvalbumin-positive (PV), somatostatin-positive (SST) or vasoactive intestinal peptide-positive (VIP) interneurons<sup>10,11</sup>, which modulate their emergence as well as other dynamic properties of circuits<sup>12–16</sup>.

The functions of fast neural oscillations are less clear. Evidence from electrophysiological recordings traditionally established fast oscillations as a plausible mechanism for intra- and inter-areal communication<sup>2,17,18</sup>, with recent work broadening or challenging the idea<sup>5,19–21</sup>. For example, computational models have shown that frequency-dependent inter-areal coherence can be enhanced without rhythmic input to neural circuits<sup>20</sup>. This questions the potential importance of neural oscillations for communication<sup>21,22</sup> although the presence of neural oscillations seems to enhance communication with respect to non-rhythmic communication<sup>20</sup>. Human noninvasive recordings have established a link between alpha/low beta rhythms in occipital cortex and local inhibition<sup>23,24</sup>, but it is uncertain whether oscillations are the cause or consequence of such inhibition. Due to the relative ease with which oscillations arise in neural circuits and the lack of a clear functionality, it is difficult to discern whether oscillations are simply a byproduct of canonical neural circuits or whether they are linked more fundamentally to brain function. Characterizing which conditions, beyond those present in canonical circuits, are necessary for the emergence of rhythmic activity is a key step in this process.

Here, we tackle the above question by building a biologically detailed model of a cortical column of mouse primary visual cortex V1 and studying the emergence of rhythmic activity in it. Our model incorporates dynamic properties of multiple postsynaptic receptors (AMPA, NMDA, and GABA-A receptors), and is tightly constrained by state-of-the-art cortical connectivity data<sup>25–28</sup>, which include cell densities and laminar-specific connectivity patterns across four different cell types (pyramidal neurons and PV, SST and VIP interneurons<sup>10,11</sup>) and five laminar modules (layers 1, 2/3, 4, 5 and 6). We first fitted the parameters of the model, in particular the global coupling strength and the external background currents, to match and replicate spontaneous and stimulus-evoked firing rates *in vivo*<sup>27,28</sup>, extending previous cortical column models which were limited to two cell types<sup>27,29</sup>. Rhythmic activity was notoriously absent from model dynamics, even in the presence of strong external input. However, upon introducing spike-timing-dependent plasticity (STDP), the model gave rise to broad-band (15-60 Hz) neural oscillations. These oscillations first appeared within layer 4 upon stimulating that layer via feedforward input, and then propagated to other layers as observed experimentally<sup>30</sup>. We furthermore show that (i) the frequency and power of oscillations can be respectively up or down-modulated via feedforward or feedback input to the cortical column, (ii) all interneuron types participate in the generation of fast oscillations, with PV cells playing a major role, and (iii) oscillations are not obtained when we artificially increase the synaptic strength, but are rather a consequence of selective, pairwise reinforcement of synapses due to experience-dependent plasticity. Our results demonstrate that neural oscillations are not simply a byproduct of having realistic connectivity patterns in canonical cortical columns, and that their appearance reflects underlying circuit reconfigurations due to synaptic plasticity. Thus, the functionality of oscillations is not bounded by having a realistic connectivity of cortical columns per se, but by selective and distributed experience-dependent plasticity.

## **Results**

We begin by describing our cortical column model, sketched in Fig. 1. We consider a network of 5,000 spiking neurons which are distributed across five laminar modules, four of which (layers 2/3, 4, 5 and 6) contain pyramidal neurons as well as PV, SST and VIP cells, and one of which (layer 1) contains only VIP cells. For laminar modules with multiple cell types,

about 85% of the cells are pyramidal neurons and the remaining 15% are inhibitory interneurons –with the precise proportion of each inhibitory cell type in each layer given by anatomical data<sup>28</sup> and depicted in Fig. 1 as the relative size of the respective inhibitory population (see Supplementary Tables 1 and 2 for more information). To establish the overall *connection strength* between any two populations, we combined the average synaptic strength with the connection probability taken from experimental measurements<sup>28</sup>. Besides the input from other neurons within the column, each neuron also received a background noise, generated by a Poissonian generator specific to each cell (Table S9). Neurons were specified as current-based leaky integrate-and-fire (LIF) models with dynamic variables for AMPA, GABA and NMDA receptors (see Methods).

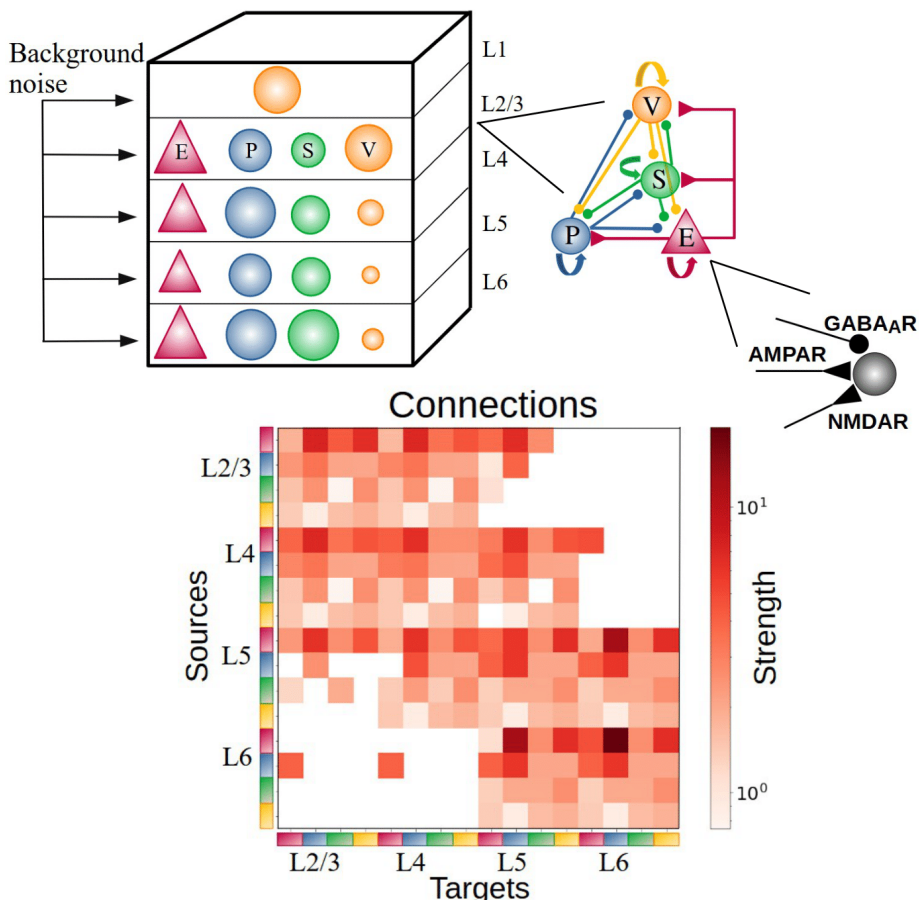
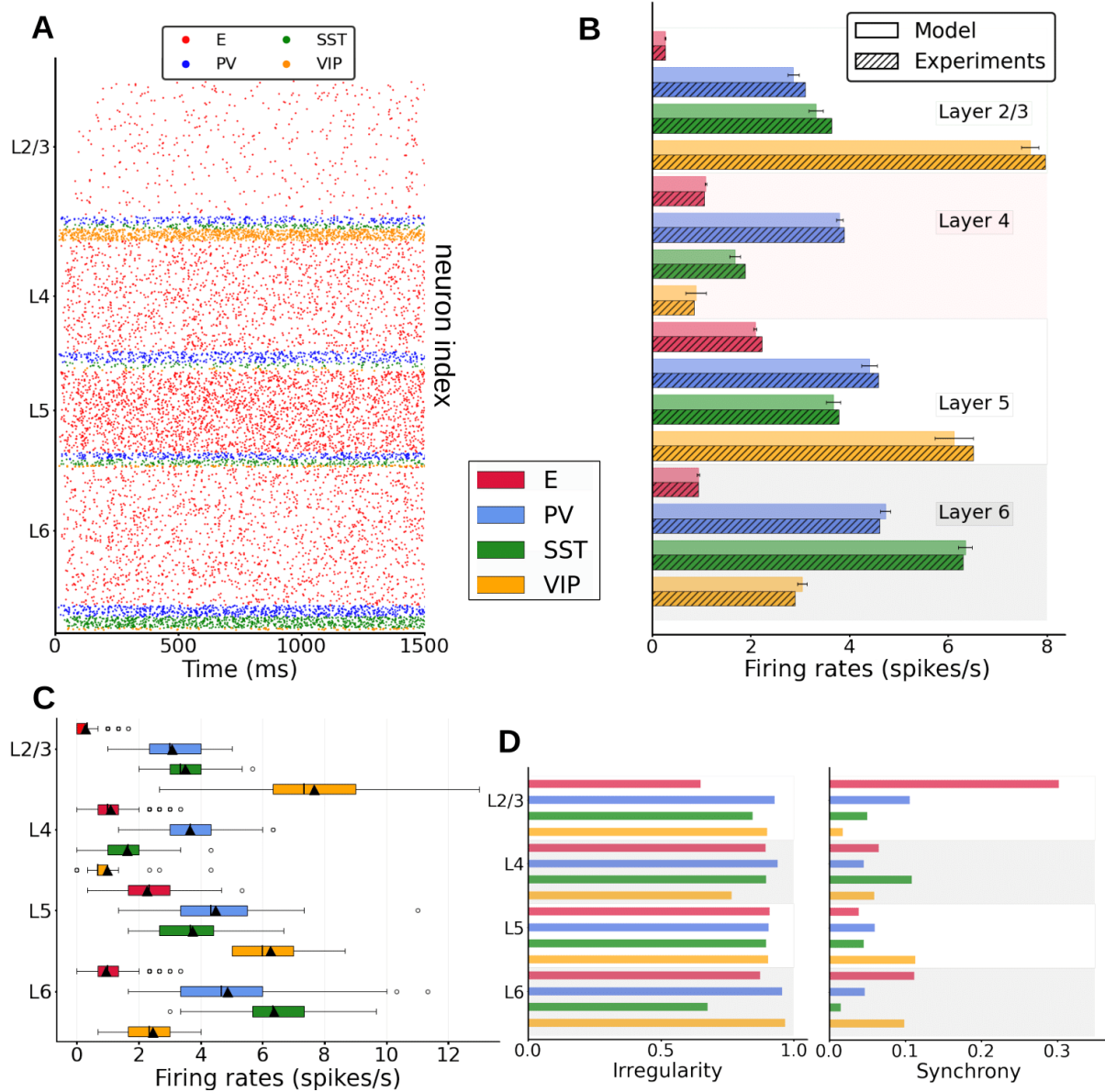


Figure 1: Sketch of the cortical column model. In layers 2/3, 4, 5, and 6 an excitatory population E, (red triangles) and 3 types of inhibitory population (PV, SST, VIP as blue, green, orange circles: P, S and V, respectively) are present. In layer 1 only VIP cells are present. The size of the circles in the top-left panel represents the relative size of the inhibitory populations. Connections between groups are not explicitly shown in the top left diagram; the zoomed-in schematic to the right shows inter-population connectivity and postsynaptic receptors (AMPA, GABA, NMDA) involved. The connectivity matrix is shown at the bottom (adapted from previous work<sup>28</sup>).

### Spontaneous cell type and layer-specific activity

To match the spontaneous firing rates of all cell types observed *in vivo*, we adjusted the global scaling value for the entire connectivity and the cell-specific background inputs to the column, similar to previous work<sup>27,29</sup>. The resulting simulated spontaneous spiking activity in the cortical column is displayed as a raster plot in Fig. 2A. For all cell types in our model, asynchronous irregular activity patterns were obtained, with firing rate levels matching quite closely those observed *in vivo* (Fig. 2B). The activity varied significantly across layers and cell types. Across all layers, pyramidal neurons exhibited the lowest firing rates in their laminar module, with mean firing rates around 2 Hz for layer 5 and below or close to 1 Hz for other layers, in agreement with experimental data<sup>28</sup>. In all layers, firing rates of inhibitory cells exceeded those of excitatory cells, except for VIP cells in layer 4. This sets the columnar model in an inhibition-dominated regime with a basal pattern of asynchronous firing<sup>31</sup>.

In addition to the heterogeneity in firing rates found between layers and cell types, single-neuron firing rates within the same population also displayed substantial variability (Fig. 2C). For example, some pyramidal neurons in layer 2/3 fired at 2 Hz, while the majority of them were rather quiescent, emitting less than one spike per second. This is in agreement with previous findings<sup>27</sup>. Overall, single-unit activity was quite irregular, with the mean of the single-unit coefficients of variation of the inter-spike intervals of all cell types being >0.5 (Fig. 2D, left panel) and membrane potential traces<sup>32</sup> displaying a rather marked asynchrony, measured using standard procedures<sup>32</sup>.



*Figure 2: Spontaneous cell-type specific activity in the columnar model. (A) Raster plot of spiking activity simulated for 1500 ms in layers 2/3, 4, 5, and 6 (see inset for cell types). (B) Mean firing rates for each model population (full bars, standard deviation computed over 10 network realizations or initializations) vs experiment (dashed bars). (C) Boxplot of single-unit firing rates in the model. Circles show outliers, black triangles indicate the mean firing rate of the population, and black vertical lines in each box indicate the median. (D) Left: Irregularity of single-unit spike trains quantified by the coefficient of variation of the inter-spike intervals. Right: Synchrony of multi-neuron spiking activity quantified by membrane potential traces.*

Because the role of inhibitory neurons is crucial to control the level of firing activity in the columnar model, we analysed the effects of inactivating different interneuron populations. As shown in Fig. S1, the activity of all neurons drastically rose when inhibitory neurons were shut down. In particular, we blocked the transmission of signals from inhibitory to all other

neurons, resulting in a sharp increase in pyramidal cell firing rates, which in turn drove the inhibitory firing rate up (even though this firing of inhibitory neurons was not able to suppress the columnar activity).

We controlled for the size of the cortical column model, as it has been reported that not all measurements in spiking columnar models scale linearly with network size and finite-size scaling studies must be performed<sup>29</sup>. When increasing the size of the network in our model and rescaling the weights accordingly (see Methods), we obtained the same firing rate statistics for sufficiently large networks. In Fig. S2, we show the mean firing rates of spontaneous activity using a network of 5,000 neurons, a network of 10,000 neurons, and a network of 20,000 neurons, with similar results in all cases.

### **Stimulus-evoked responses of the column**

Once the model parameters were fitted to reproduce spontaneous activity, we tested its response to feedforward stimuli mimicking a simple sensory signal. Confronted with a feedforward thalamic input arriving to layer 4, the columnar model responded with a stereotypical rise and propagation of activity through different layers. Fig. 3A shows an example raster plot of the model when a constant input was given to all pyramidal neurons in layer 4. Pyramidal cells in layers 2/3, 4 and 6 considerably increased their relative activity in response to the stimulus, while those in layer 5 showed a weaker response. Fig. 3B shows the mean firing rates as the input arrives to layer 4 pyramidal cells. Both excitatory and inhibitory populations displayed a significant increase in firing rate due to the input. Inhibitory neurons played a substantial role in how the signal was propagated throughout the column. For example, the reason why pyramidal neurons in layer 5 might respond so weakly to layer 4 input is the PV cell activation in layer 5, where this activity increased significantly (compared to most other inhibitory cell types in other layers) and prevented a further increase in pyramidal neuron activity in layer 5.

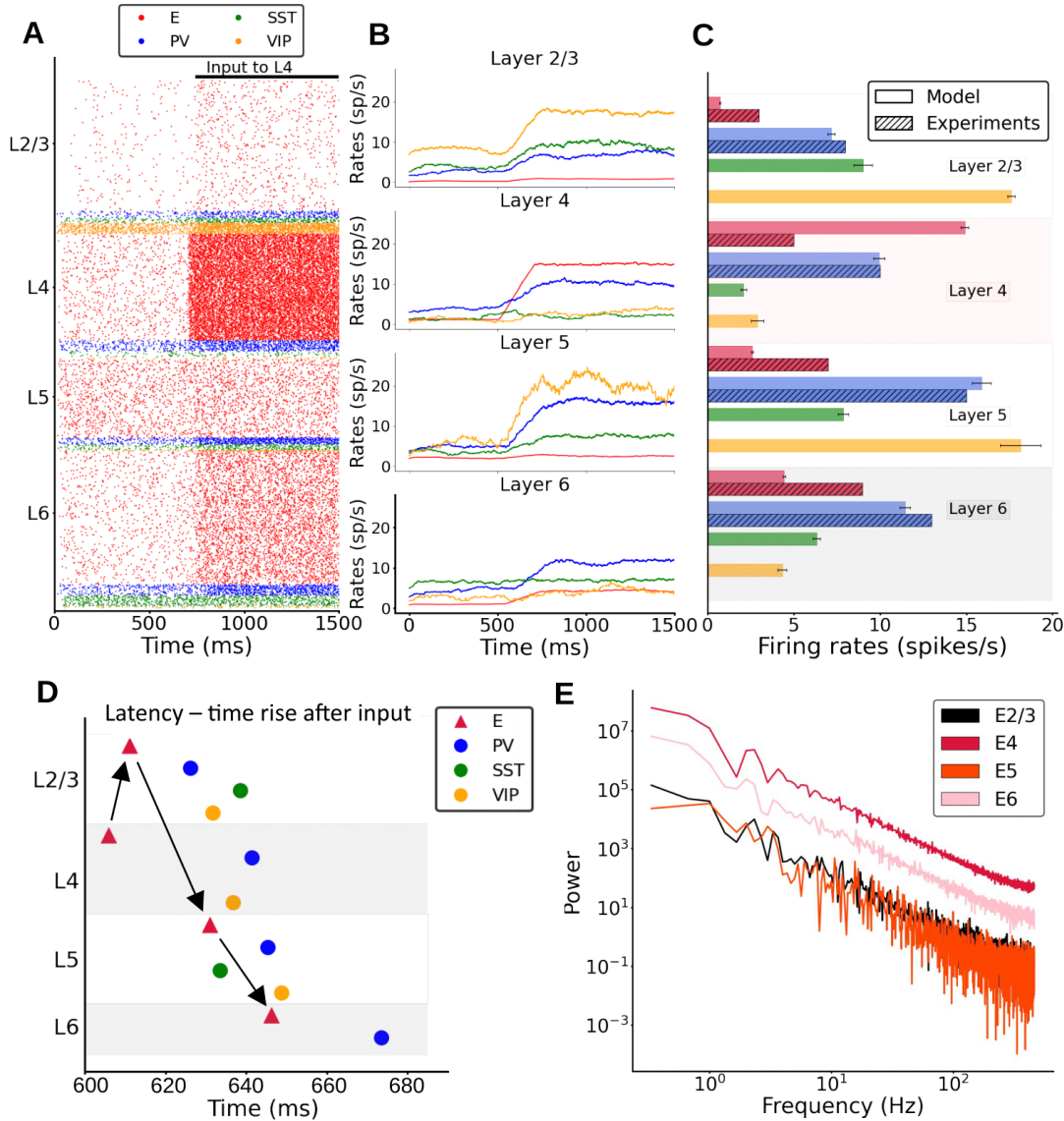


Figure 3: Stimulus-evoked cell-type specific activity in the columnar model. (A) Raster plot of spiking activity for 1500 ms showing the response of neurons after an input current (30 pA) is applied to layer 4 pyramidal neurons at 700 ms. (B) Mean firing rate traces (computed with a 200 ms sliding window and a 1-ms step) showing the increase of the overall activity when the input current is injected. (C) Mean firing rates after stimulus onset of each population for the model (solid bars) vs experimental mean firing rates (dashed bars). The error bar for the model are computed as standard deviation over 10 different simulations. Error bars for experimental data are not depicted. Boxplots of experimental firing rates can be found in Billeh et al.<sup>22</sup>, in their figure 3F .(D) Propagation order of the signal elicited by layer 4 excitatory cell stimulation. This is obtained averaging the times rise of 10 different simulations. (E) Power spectrum of excitatory mean firing rates across all layers, showing no signs of oscillatory activity.

To illustrate the power of the model in predicting responses to feedforward stimuli, Fig. 3C shows the mean firing rates after the input had been activated in comparison with experimental data from mouse V1 during passive visual stimulation<sup>28</sup>. Although not

specifically fitted to reproduce stimulus-evoked activity, the columnar model performed reasonably well and provided good firing rate estimations for all PV interneurons as well as pyramidal neurons (falling within one standard deviation of the experimental range<sup>28</sup>). Experimental data on the evoked activity of SST and VIP cells were not available, therefore the results in Fig. 3D may serve as model predictions for future studies.

After the feedforward input excited pyramidal neurons in layer 4, the signal propagated to layer 2/3, then 5 and finally to layer 6 pyramidal cells – generating the sequential activation pattern in canonical microcircuits as proposed in classic neuroanatomical studies<sup>33,34</sup>. This was not captured by previous cortical models<sup>27,29</sup>, which indicates that explicitly considering the role SST and VIP neurons is important to understand feedforward activation in the cortical column. The order of responding is clearly shown in Fig. 3D, which shows the activation latency of each population, quantified as the time at which each population reached half of its maximum evoked firing rate. In each layer, the cell type activated first was the pyramidal neuron, followed by inhibitory interneurons after a certain delay, caused by the smoother ramping of inhibitory activity in general. Notably, while the order of activation is the same for pyramidal, PV and VIP cells (layer 4 to 2/3 to 5 to 6), SST cells display a different activation trajectory – increasing their firing rate first on layer 5 and shortly thereafter in layer 2/3, while remaining at spontaneous levels in layer 4 and 6. This suggests that activation patterns in canonical cortical circuits are specific to cell types. The difference in activation latency between the input layer and the deep output layers in our columnar model was about 40 ms, with variations depending on cell type.

While activity in the spontaneous condition was quite irregular (Fig. 2D) as in experimental observations, experimental evidence suggests that rhythmic activity in the range of beta (15-30 Hz) or gamma (30-70 Hz) oscillations is often evoked by visual stimulation. We analyzed the temporal evolution of firing rates across all layers in our model and found, however, no evidence of rhythmic activity (Fig. 3E) under a variety of parameter settings, i.e. different external input strengths or sizes of the network. This suggests that the emergence of neural oscillations might require more conditions than explored thus far.

## Introducing synaptic plasticity

After replicating spontaneous activity statistics, our columnar model predicted stimulus-evoked firing rates across cell types and layers, and provided a mechanistic intuition on well-known properties of cortical functioning such as microcircuit communication pathways<sup>33</sup> and gain control by deep layers<sup>35</sup>. However, so far rhythmic activity was notoriously absent, particularly for stimulus-evoked conditions (Fig. 3E) which would be expected to display stimulus-induced fast oscillations as experimentally observed<sup>36–38</sup>. It is therefore possible that oscillations do not emerge directly from the canonical network of a ‘naive’ cortical column but rather reflect more detailed, experience-dependent changes.

To test this hypothesis, we introduced synaptic plasticity in all excitatory weights of the cortical column model, via the spike-timing-dependent plasticity (STDP) rule (Fig. 4A). To drive long-lasting changes in columnar connectivity, we applied a constant feedforward input arriving at half of the pyramidal neurons in layer 4. Each synaptic weight was initialized as in the results described above. Incorporating STDP resulted in changes in the spiking activity across the column, which evolved from an asynchronous, irregular regime (Fig. 4B, left plot) to a regular, oscillatory pattern only after the plasticity rule led to changes in synaptic strengths (Fig. 4B, middle and right plots). These fast, low-gamma (~26 Hz) oscillations emerged within ~55 seconds after STDP was enabled, due to strong, continuous input to layer 4 pyramidal cells—although lower learning rates extended this time window considerably. Rhythmic neural activity was present from then on across all layers, with layer 4 displaying the strongest power in the low-gamma frequency band (Fig. 4C). It engaged all cell types to various degrees, as evidenced by firing rate traces (compare e.g. left and right traces in Fig. 4D, corresponding to moments before and after strong changes in the synaptic weight were induced by the STDP rule).

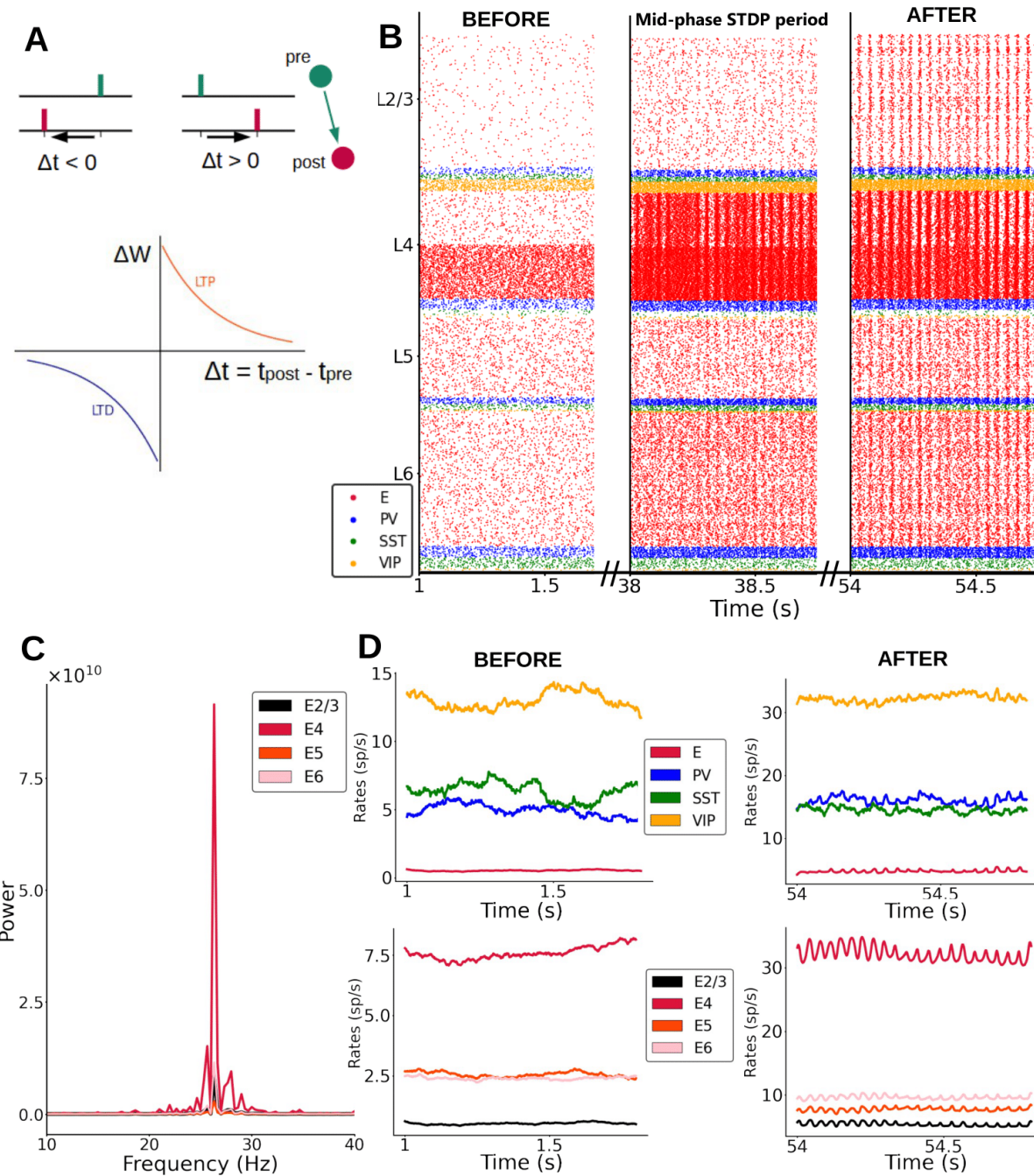


**Figure 4: Synaptic plasticity gives rise to fast oscillations.** (A) Scheme of STDP rule, with reductions vs increases in excitatory synaptic strength (excitatory-excitatory synapses only) driven by pre- and post-synaptic spike timing.  $\Delta t$  is the time between pre and post synaptic spike of a pair of connected neurons.  $\Delta W$  is the change of synaptic weight of the pair according to the STDP rule, LTP stands for long term potentiation and LTD for long term depression (B) Raster plot of spike activity in the column at three example episodes from the plasticity period (1 s, 38 s, 54 s; this period starts at 0 s) showing the emergence of oscillations after instantiating plasticity. An input of 30 pA (from  $t=0.5$  s onwards) is given to half of the pyramidal cells in layer 4 and all excitatory-to-excitatory connections in the entire column evolve according to the STDP rule. (C) Power spectrum of the firing rates of pyramidal cells for different layers. The oscillations of pyramidal activity at the end of the plasticity period (55s) have a mean frequency of 26 Hz for an input of 30 pA. (D) Firing rate traces at the beginning (left) and at the end (right) of the plasticity period. Top row: rates in layer 2/3 for all four neuron types. Bottom row: rates of excitatory neurons in all layers.

### Oscillatory frequency and amplitude are modulated by feedforward and feedback input

Once the plasticity period was over (55 s), weights were fixed to study the resulting dynamics as a function of input strength. We observed that oscillations were triggered and maintained by the feedforward input, and as soon as the input was switched off, the oscillations faded away and activity returned to spontaneous baseline levels. If the input was switched back on, the oscillations automatically reappeared (Fig. S3). Similar to experimental observations with varying visual contrast<sup>36–38</sup>, the strength of the external input to layer 4 pyramidal cells modulated the frequency and amplitude of the resulting oscillations (Fig. 5A and S4). As the input strength increased, the oscillatory frequency rose from 15 Hz up to 60 Hz (Fig. 5B). The oscillatory power exhibited an inverted-U relationship as a function of the input (Fig. 5C). The effect of (presumably feedback) input to layer 5 had the opposite effect: increasing input strength to layer 5 pyramidal cells (while keeping a constant input to layer 4) led to a reduction in layer 4 pyramidal oscillatory activity, with the reduction being proportional to the strength of input to layer 5 (Fig. 5D and S5). Overall, excitatory input to layer 5 pyramidal cells led to a decrease of oscillatory frequency in all layers except in layer 5, where it increased with input strength (Fig. 5E) and to an overall reduction of oscillatory power across the entire column (Fig. 5F). Thus, feedback input had a strong dampening and slowing effect on the oscillations. Interactions between feedforward and feedback input are therefore able to precisely modulate the rhythmic components of cortical activity.

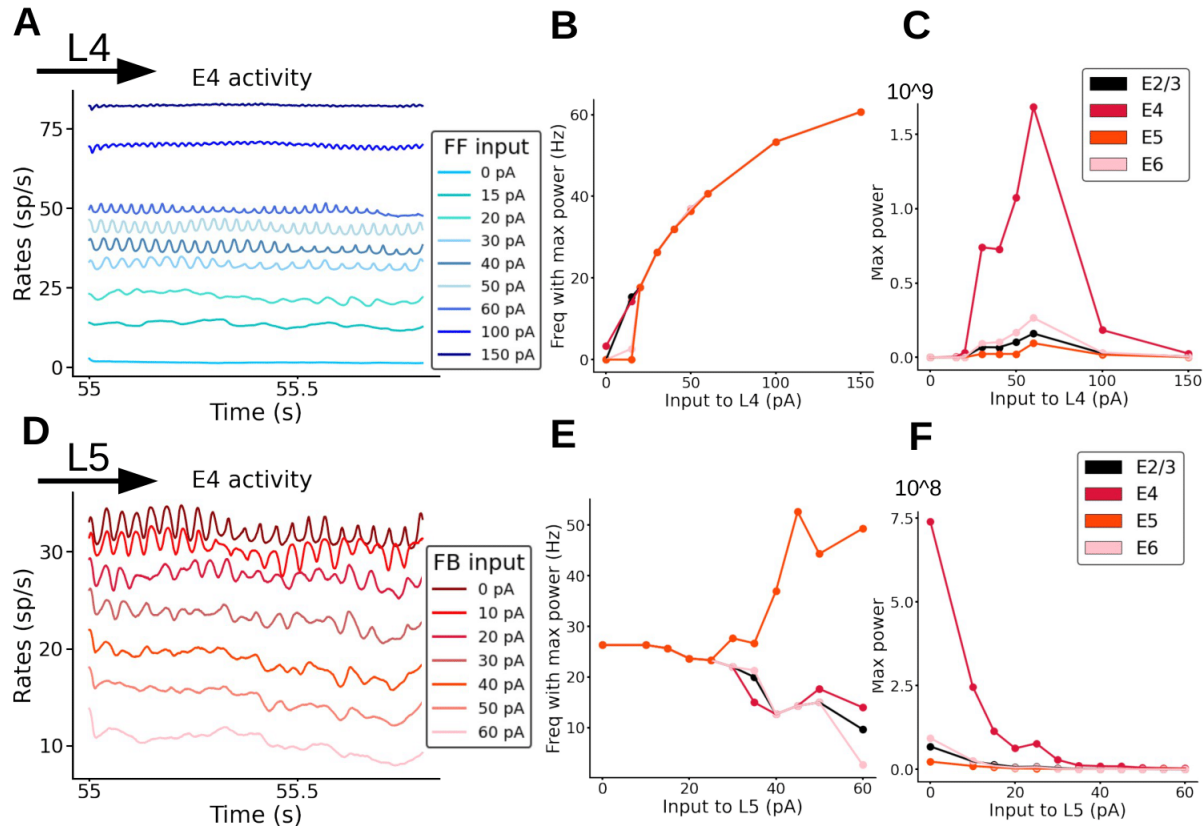


*Figure 5: Fast oscillations are modulated by external input. (A-C) . Modulation of oscillations of excitatory neurons in layer 4 (E4) by feedforward (FF) input strength. (A) Firing rates of excitatory neurons in layer 4, each color represents a simulation with a different input strength (color code in inset). The stronger the input to layer 4, the faster the oscillations are (dark blue trace). When no input to layer 4 is present the oscillations disappear (light blue trace; 0 pA). (B) Frequency of firing rate of excitatory neurons in all layers as a function of input strength to layer 4. (C) Maximal power of oscillations as a function of input strength to layer 4 (D-F) Modulation of oscillations of excitatory neurons in layer 4 by feedback (FB) input strength, while input to layer 4 is kept constant. (D) Firing rates of excitatory neurons in layer 4, each color represents a simulation with a different input strength to layer 5, (color code in inset). The stronger the input to layer 5, the slower the oscillations are. When the input strength to layer 5 is very high (60 pA) the oscillations disappear (pink trace). (E) Frequency of oscillatory activity of excitatory neurons as a function of the input to layer 5. (F) Maximal power of oscillations as a function of the input strength to layer 5.*

### Origin of cortical oscillations

To better understand the relationship between synaptic plasticity and oscillations as suggested by our cortical column model, it is important to study the mechanisms giving rise to the observed oscillations. Our first aim in this sense was to find out whether oscillations emerge globally and simultaneously across the entire column, or whether a subcircuit directly mediated its generation, driving the rest of the columnar network. A candidate for such a driver role is the layer 4 microcircuit, as it receives the feedforward input initiating

experience-dependent processing and has been identified as a gamma generator within visual columns<sup>30</sup>.

When the STDP rule was applied to all excitatory-to-excitatory synapses in the column, the column displayed fast oscillations after a plasticity period as before (Fig. 6A, panel A1). We then repeated the process by allowing STDP-mediated changes in all excitatory-to-excitatory synapses except for those from layer 4, resulting in a network in which oscillations were absent after the plasticity period (Fig. 6A, panel A2). We repeated the process once again, this time only allowing plasticity in excitatory synapses from layer 4. This was sufficient to drive oscillations in all layers (Fig. 6A, panel A3), suggesting that plasticity in the efferent connections from layer 4 is crucial for cortical rhythmicity and that the efferents from layer 4 are the main generator of fast oscillations –which later propagate to other layers, in agreement with experimental data<sup>30</sup>. This also suggests that plasticity in excitatory outputs from layer 2/3, 5 and 6 cells is not crucial for oscillations: without plasticity in these connections oscillations are still emerging.

To analyze which groups (i.e. a given cell type in a given layer) of interneurons are crucial for the emergence of oscillations, we investigated the effect of inactivating different types of interneuron in the whole column. Fig. 6B shows the raster plots for five different conditions, from left to right: (i) the control condition, and inactivation of (ii) SST cells only, (iii) VIP cells only, (iv) PV cells only, and (v) all inhibitory neurons. Inactivating PV cells had the largest effect amongst specific interneuron inactivations, leading to a sharp increase in the oscillatory frequency across the entire column. Inactivating SST or VIP cells had similar, but much more modest effects on the oscillations. Removing specific groups of interneurons in specific layers led to increases in oscillation frequency (Fig. S6-S10), with the notable exception of layer 5: inactivating interneuron groups in that layer drastically reduced the power of oscillations in other layers, due to the link between layer 5 pyramidal activity and column-wide rhythms (Fig. S7).

Importantly, the more groups we inhibited, the more the oscillation behaviour was influenced. In Fig. S6 we show that removing only one inhibitory group in layer 4 increases the oscillations frequency slightly, with PV4 having the biggest effect. However, the removal

of only one group is not enough to drastically change the frequency of oscillations (Fig. S6). In contrast, silencing more groups at the same time increased the oscillation frequency significantly (Fig. S7). Fig. S8 shows that inhibitory neuron groups in each layer are contributing to oscillations in the whole column , in fact the effect of silencing inhibitory neurons is similar for the different layers (removing inhibition from L2/3 vs L4 vs L6). With these analyses (and more not shown) we can conclude that all inhibitory neuron groups (PV, SST, VIP) make a contribution to maintain oscillations; all of them are relevant even though to different extents (PV being the most important). To further test the relevance of PV interneurons, we silenced all inhibitory groups except one type. Fig. S9 shows that when all inhibitory neuron types except PV are silenced (in all layers ), oscillations are still present, thus PV cells alone (but coupled to pyramidal cells) are able to maintain oscillations. In this case the oscillations became slightly faster because of the absence of SST and VIP cells. The same behaviour was not observed when SST or VIP cells were present alone, in this case oscillations were expressed at a much higher frequency. This suggests that, while all interneuron types participate in the generation of oscillations, PV cells appear to be more relevant than SST or VIP cells<sup>39</sup>. Given the important role of PV cells we investigated this further and in Fig. S10 we show how the frequency of oscillations can be modulated by applying differential external input to PV cells in layer 4. The more input current was applied, the slower the oscillations became.

After gaining insight in the full columnar model, we next focused on an isolated subcircuit of layer 4, given its crucial role in rhythm generation. Specifically, we isolated the layer 4 subcircuit by removing all its incoming and outgoing connections with other parts of the column, this was done after the plasticity period had been applied to the entire column from  $t = 0$  until 55 s. This subcircuit was still showing oscillations, although the rhythmicity was not as clear as for the full column. The omission of inhibitory connections from the other layers resulted in faster oscillations: 37 Hz (compared to the full column case: 26 Hz) and a higher firing rate activity. We then inactivated (or silenced) one inhibitory population at a time to observe its effect on oscillatory behavior. As in the full-column model, we found a particularly strong effect when inactivating layer 4 PV cells, as this severely disrupted oscillations (Fig. 6C and S11). Likewise, inactivating all types of layer 4 interneuron had a strong impact in terms of drops in power, while inactivating SST and VIP cells had only a

slight to moderate impact. To test that the impact of PV cells was not due to the higher number of PV cells with respect to SST cells, we also inactivated a subpopulation of PV cells (PV-sub), equal in size to the number of SST neurons in layer 4 (i.e., the largest group of layer 4 inhibitory cells after PV cells), and the results were similar to the inactivation of the full PV population (this was also verified in the full column case, see S13). The prominent role of PV cells appeared to be related instead of their higher number to the synaptic connections from PV to pyramidal neurons, which are stronger than projections from SST to pyramidal neurons, given the preference of PV cells to establish synapses on pyramidal cell somata (as reflected in the connectivity strength data). Finally, inactivations did not drastically change the layer 4 oscillatory frequency in the case of SST and VIP cells, and led to higher frequencies for PV cells (Fig. 6C and S11). This suggests that, while all interneurons participate in the generation of oscillations, PV cells seem to be more relevant than SST or VIP cells.

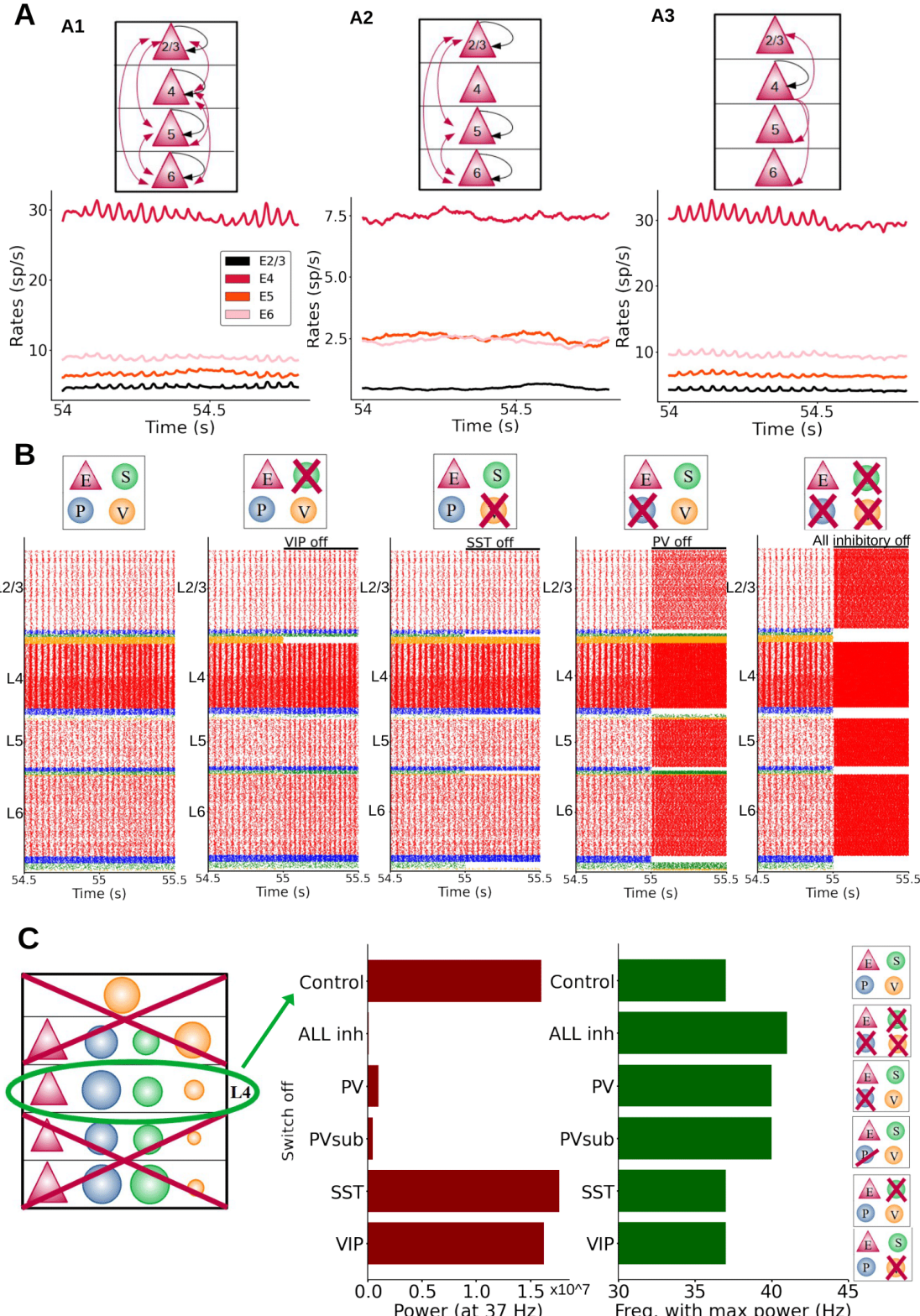


Figure 6: Mechanistic origin of oscillations. (A) Different effects on oscillations depending on the layer in which plasticity of excitatory-to-excitatory synapses is enabled. (Black arrows: plasticity within a group; red arrows: plasticity between different groups). Left: plasticity in all excitatory-to-excitatory connections. Firing rate profiles were obtained while L4 input

*was provided to half of the pyramidal cells in layer 4. Middle: plasticity in connections between all layers except those from and to layer 4. Right: plasticity enabled only in synapses from layer 4 excitatory neurons. There was no plasticity in the connections going from layer 2/3,5,6 to the other layers. (B) Raster plots of the whole column model for different inactivation conditions. Each group(s) is inactivated at 55 s, to better visualize the effects on neural dynamics. From left to right: control, inactivation of SST, VIP, PV cells and all inhibitory neurons, respectively. Inhibition of PV cells had the largest effect on oscillation frequency and amplitude. (C) Isolated layer 4 circuit. The oscillation frequency in the control situation was 37 Hz. Middle panel: oscillatory power at the 37 Hz frequency for inactivations of different cell groups: all inhibitory, PV, PVsub (same number of PV cells silenced as the number of SST cells present in the column), VIP and SST cells. Note that switching off VIP cells did not change the power of the oscillations drastically as was the case for PV inactivation. Right panel: oscillatory frequency with the maximum power for the same conditions. When switching PV cells off the oscillation frequency (with the maximum power) changed from 37 Hz to a higher value (41 Hz). . The power of the oscillations frequency is shown in S11.*

### **Importance of specific changes in the connectome for the emergence of oscillations**

While the above analyses identify some of the key ingredients for the emergence of oscillations in response to long-lasting synaptic changes, it is still unclear what aspects of plasticity are crucial for the emergence of oscillations. It could be that oscillations simply arise due to a global increase (or upscaling) of synaptic weights, or alternatively that refined experience-dependent structural changes due to plasticity play a more important role. To test this, we shuffled the synaptic weights within our cortical model after the plasticity period (Fig. 7A1), as shuffling preserves any overall increase in global coupling level, and observed the impact of shuffling on columnar dynamics. We found that shuffling led to a significant decrease in oscillatory power across all layers (Fig. 7A2 and S14), with oscillations becoming clearly weaker in layer 4 and almost vanishing from other layers such as 2/3 (Fig. 7A3). The oscillatory power at 26 Hz drops from  $\sim 7 \times 10^7$  to  $\sim 7 \times 10^2$  for excitatory neurons in layer 2/3 (See S14 for details on all layers). This indicates that specific pairwise reinforcements and the associated structural cross-correlations sculpted by synaptic plasticity are key to the genesis of oscillations.

Next we compared the dynamics of a cortical column model with synaptic weights changed due to plasticity (Fig. 7A, middle panels) with a model in which weights were increased, independent from experience-dependent plasticity. In this ‘uniformly increased’ (UI) model, excitatory connections were artificially enhanced from the naive condition to match the overall strength of connectivity of the first model, but without undergoing STDP-regulated

changes. This was done by calculating the average synaptic strength of all connections after plasticity induction, comparing this average to the average in the naive network and then increasing the synaptic strength of all connections by that same percentual change in our new UI network. As Fig. 7B shows, a simple increase in global excitatory-to-excitatory synaptic strength is not enough to induce oscillations, indicating again that a specific experience-dependent connectivity pattern and cross-correlations resulting from this pattern are required to generate oscillatory activity in our cortical column model.

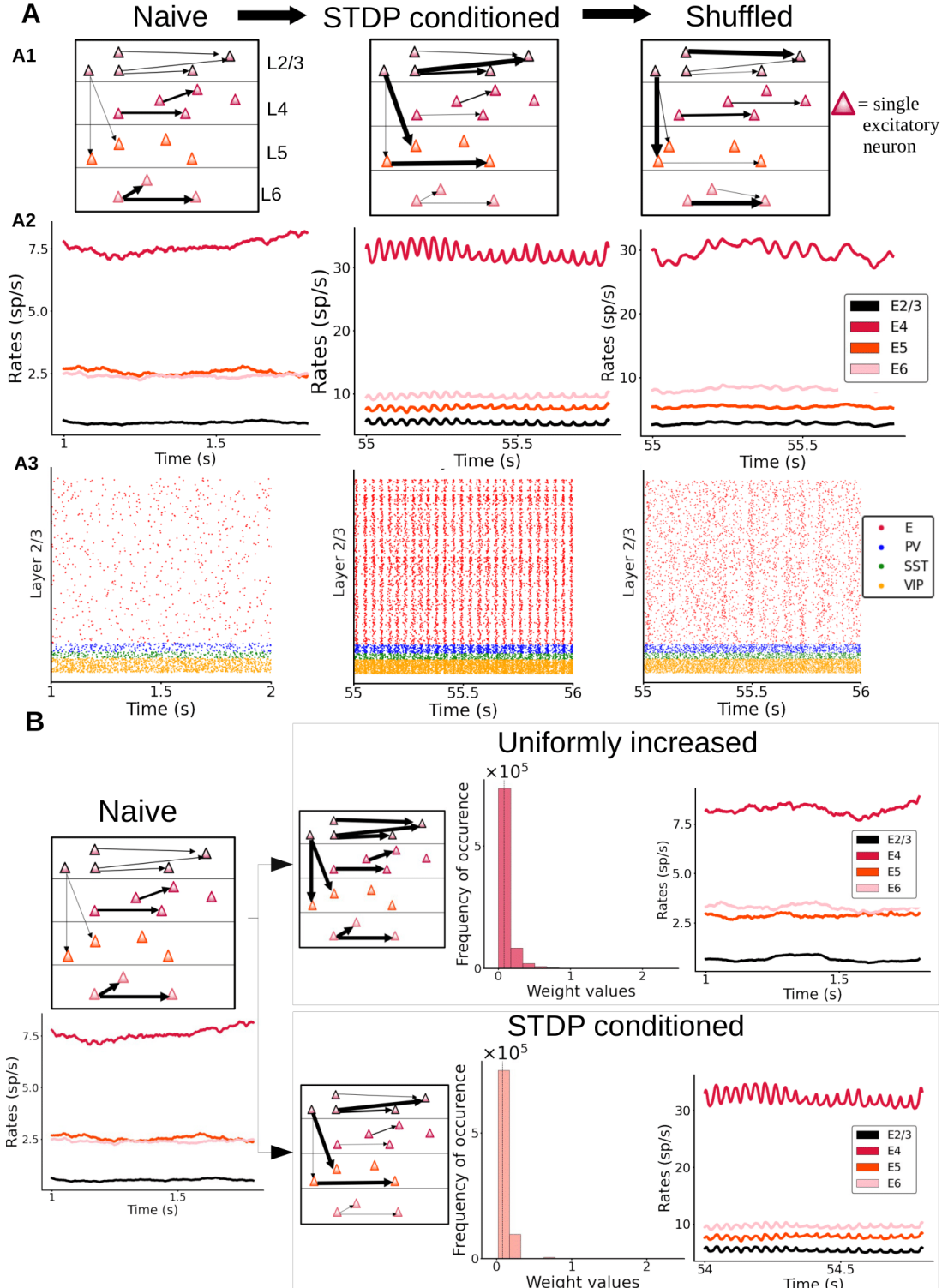


Figure 7: Importance of having a specific distribution of synaptic weights for the genesis of oscillations. (A) Left: “naive” column, prior to plasticity. Middle: columnar model after enabling synaptic plasticity, with activity driven by feedforward

*input (30 pA to half of the layer 4 pyramidal neurons). Right: same as in the middle panel, but with weights randomly shuffled between individual cell pairs. A2: Firing rate traces of excitatory cells in all layers of the three networks. A3: Raster plots for layer 2/3 are shown for all three networks. (B) A naive column (left) may be either subjected to stimulus-driven changes via STDP (bottom right) or to an equivalent mean increase of all its weights with a similar global weight distribution as the STDP-conditioned network (see histograms with probability distribution of weight values) but without STDP-sculpted structural correlations. Firing rate traces show the presence or absence of oscillations in each case.*

## **Discussion**

We built a neurobiologically detailed model of a cortical column of mouse V1, characterizing its dynamics under conditions of spontaneous activity and sensory stimulation, and exploring how oscillations may emerge in the network. Our model, first and foremost, is built upon detailed empirical datasets of cell-type-specific connectivity patterns between neurons of the visual cortex across all layers. Constraining the model with this data is of the utmost importance to arrive at accurate and relevant predictions. To complete this precise mathematical description of the V1 cortical column, and to more faithfully reproduce rhythmic dynamics and response to input<sup>7</sup>, we also implemented realistic postsynaptic dynamics for AMPA, GABA and NMDA receptors <sup>40</sup>.

For model fitting, we focused on adjusting the parameters for background currents and global coupling strength, as these parameters are difficult to estimate from in vitro recordings but are important determinants of the dynamics<sup>41</sup>, and are commonly used for fitting these type of models<sup>27,29</sup>. After the parameter adjustments, our columnar model was able to replicate in vivo spontaneous firing patterns (including mean firing rates, spiking irregularity, and synchrony measures) across all cell types and layers. Without further parameter tuning, the model was next able to provide good estimates of activity levels for stimulus-evoked conditions, which are in agreement with existing data for pyramidal and PV cells<sup>27</sup> and constitute useful predictions for SST and VIP cells. Although other models in the literature have also been able to match firing rates of excitatory and inhibitory cells under spontaneous and evoked conditions, they either did not account for interneuron variability<sup>27,29</sup>, or readjusted connectivity weights using biologically implausible optimization methods<sup>28</sup> or focused on other brain areas such as barrel cortex<sup>42</sup>. In this sense, our model constitutes perhaps the most biologically plausible model of the mouse

V1 column presented until now, particularly for understanding the effects of different types of interneuron on columnar dynamics (Figs. 6 and 7). This also opens the door to use our cortical column model to study the effects of heterogeneity within the same class of cells, using for example existing mean-field approaches<sup>43,44</sup>.

Our model demonstrated a substantial level of agreement with experimental evidence. Aside from the realistic cell- and layer-specific spontaneous and stimulus-evoked firing statistics, the model successfully replicated a number of experimental observations. First, feeding a feedforward signal to the columnar model triggered the sequential activation of different layers, as predicated by canonical microcircuit diagrams<sup>33,34</sup>. Because previous columnar models without different interneuron types did not show this pattern, this indicates that SST and VIP cells seem to play a role in this translaminar signal propagation – potentially relying on the benefits of interneuronal heterogeneity for signal transmission in cortical circuits<sup>43,44</sup>. Our model predicts a dependence on SST and VIP cells which can be experimentally tested by optogenetic inactivation. Second, activating pyramidal neurons in layer 5 had an inhibitory effect on other layers, particularly layer 2/3, in agreement with previous observations<sup>45</sup>. Third, after synaptic plasticity was enabled, feedforward input was able to generate fast oscillations, first in layer 4 and later in other layers. This temporal laminar sequence has in fact been experimentally observed<sup>30</sup>. Fourth, strong feedforward input increased the power and frequency of oscillations<sup>36–38</sup>. Fifth, feedback input suppressed fast oscillations or reduced their power, as observed *in vivo* in V1 recordings<sup>30</sup>.

Besides the generation of the model itself and its validation with existing data, our work reveals a fundamental property of cortical columnar circuits in generating neural oscillations. The finding that fast oscillations are a direct reflection of experience-driven changes in cortical circuits confronts traditional ideas in the field. Concretely, given that rhythmic activity is ubiquitous in the brain, and that synchrony can be easily obtained in abstract computational neuroscience models, it is sometimes assumed that oscillations naturally arise in canonical neural networks without involvement of experience-dependent plasticity and the fine connectivity structure it entails. Only by carefully addressing the question with a data-constrained columnar model, as done here, one may reveal the vital role that experience-dependent structural pairwise interactions have on generating cortical

rhythmic dynamics. This aligns well with existing ideas which link fast oscillations to flexible mechanisms for the development of cognitive function, such as co-optation mechanisms<sup>1</sup>. On the other hand, increasing the strength of all excitatory synapses to high levels in our model would also be expected to lead to oscillations without STDP – synchrony is, after all, an emerging property of networked excitable systems. However, when our model was subjected to STDP, excitatory synapses tended to be weak overall (for example compared to inhibitory neurons), so such a solution, while valid for simple models, does not seem to generalise to more realistic cortical column models.

Finally, we make several experimental predictions based on the results of our model. Regarding the activity of different cell types, alternative canonical sequential activations should exist in the V1 column when looking at different interneuron types –for example, upon stimulus onset SST cells will be activated sequentially from deep to superficial layers, while PV and VIP cells will follow the classical sequence just like pyramidal neurons (Fig. 3D). As concerns synaptic plasticity, we predict that plasticity in synapses originating in layer 4 (and targeting other cells inside and outside that layer) will be fundamental for the generation of oscillations in cortical circuits (Figure 6A). Localized pharmacological inactivation of synaptic plasticity mechanisms in layer 4 should reveal important alterations in experience-dependent rhythmic patterns. Although we have not explicitly focused on the role of NMDA receptors in columnar dynamics, the model could be used in future work to study the relationship between pharmacological blocking of NMDARs and alterations in gamma oscillations<sup>46,47</sup>, or the interaction between NMDAR and different cell types in novel paradigms of working memory<sup>45,48,49</sup>.

Overall, our biologically realistic, data-constrained cortical column model suggests a clear link between experience-dependent plastic changes and the emergence of neural oscillations. These oscillations are not present anymore if synaptic weights are randomized after learning, and simply upscaling the values of all excitatory synapses in the non-STDP model is also not enough to obtain them. In realistic columnar models, a subtle, self-organizing distributed process driven by experience is needed to produce oscillations.

## Methods

### Model architecture

The cortical column model, shown in Fig. 1, is composed of a total number ( $N_{\text{total}}$ ) of 5,000 neurons. The model consists of four cortical layers each containing pyramidal neurons, PV, SST and VIP cells (layers 2/3, 4, 5, 6) and one layer containing only VIP cells (layer 1). Each of the four ‘complete’ layers harboured pyramidal neurons (85% of cells) and inhibitory interneurons (15%; each inhibitory group in a given layer was represented by a particular percentage out of this 15%). The fractional sizes of neuron types in each layer (of the total number in the column) and those of each cell type in each layer were taken from the Allen Database<sup>28</sup> and are reported in Supplementary Tables 1 and 2. All neurons received background noise from the rest of the brain as shown in Fig. 1. The levels of background noise that each type of cell received can be found in Supplementary Table 9, the tuned spontaneous firing rate effectuated by the Poissonian spike generators connected to each group differed amongst cell types.

We use the term *connection* with reference to subpopulations or groups, defined by the pre- and postsynaptic neuron types in each layer. The connection probability defines the probability for each possible pair of pre- and postsynaptic neurons to form a connection between them. If  $p=0.1$  this connects all neurons pairs of the two groups with a probability of 10%. The connectivity probability matrix  $P$  is defined by the  $16 \times 16 + 16 \times 2 = 288$  connection probabilities  $p$  between the 17 considered cell groups (4 types in each of the 4 layers plus 1 group in layer 1; a group thus potentially receives inputs from the other 16 cell groups and also potentially projects to all of them). The connection probability matrix  $P$  used to constrain the model is available in the portal of the Allen database available at <https://portal.brain-map.org/explore/models/mv1-all-layers>. Each connection has also a particular strength which differs per neuron group. Thus, the strength was specified at the level of neuron type X projecting to neuron type Y. The strengths of connections between neurons are constrained using the matrix  $S$  available at <https://portal.brain-map.org/explore/models/mv1-all-layers>. How we set the strengths of single synapse using the matrix  $S$  is explained above (Eq. 11).

Here an example of how two groups (X and Y) are connected: VIP cells in layer 1 (X) that have a connection going to SST cells in layer 4 (Y) will all have the same connection strength. However, not all VIP cells in layer 1 are connected to SST cells in layer 4 because they connect with probability  $p$ .

### Model for neurons

All pyramidal cells and all three types of interneuron are modelled as leaky integrate-and-fire neurons. Each type of cell is characterized by its own set of parameters: a resting potential  $V_{rest}$ , a firing threshold  $V_{th}$ , a membrane capacitance  $C_m$ , a membrane leak conductance  $g_L$  and a refractory period  $\tau_{ref}$ . The corresponding membrane time constant is  $\tau_m = C_m/g_L$ . The membrane potential  $V(t)$  of a cell is given by:

$$C_m \frac{dV(t)}{dt} = -g_L (V(t) - V_{rest}) + I_{syn}(t) \quad (\text{Eq. 1})$$

where  $I_{syn}(t)$  represents the total synaptic current flowing in the cell.

At each time point of simulation, a neuron integrates the total incoming current  $I_{syn}(t)$  to update its membrane potential  $V(t)$ . When the threshold  $V_{th}$  is reached a spike is generated, followed by an instantaneous reset of the membrane potential to the resting membrane potential  $V_{rest}$ . Then, for a refractory period  $\tau_{ref}$ , the membrane potential stays at its resting value  $V_{rest}$  and no spikes can be generated. After  $\tau_{ref}$  has passed, the membrane potential can be updated again (see Tables S4-S8 for the corresponding parameter values).

### Model of synapses

Each cell group in each layer is connected to all the other groups of the cortical column with its own synaptic strength and probability. The values in matrix  $P$  indicate the probability that a neuron in group A (e.g. a PV cell in layer 4) is connected to a neuron in group B (e.g. a SST cell in layer 5). Excitatory postsynaptic currents (EPSCs) have two components mediated by AMPA and NMDA receptors, respectively. Inhibitory postsynaptic currents (IPSCs) are mediated by GABA<sub>A</sub> receptors.

The inputs to model neurons consist of three main components: background noise, external (e.g. sensory) input and recurrent input from within the column. EPSCs due to background noise are mediated in the model exclusively by AMPA receptors ( $I_{ext,AMPA}(t)$ ) and EPSCs due to external stimuli (i.e. originating from outside the column) are represented by  $I_{ext}(t)$ . The recurrent input from within the column is given by the sum of  $I_{AMPA}(t)$ ,  $I_{NMDA}(t)$ ,  $I_{GABA}(t)$ . These are all the inputs from all the other presynaptic neurons projecting to the neuron under consideration.

The total synaptic current that each neuron receives is given by:

$$I_{syn}(t) = I_{ext}(t) + I_{ext,AMPA}(t) + I_{AMPA}(t) + I_{NMDA}(t) + I_{GABA}(t) \quad (\text{Eq. 2})$$

with the last four terms given by

$$I_{ext,AMPA}(t) = g_{AMPA}(V(t) - V_E) s_{ext,AMPA}(t) \quad (\text{Eq. 3})$$

$$I_{AMPA}(t) = g_{AMPA}(V(t) - V_E) \sum_{j=1}^N w_j s_j^{AMPA}(t) \quad (\text{Eq. 4})$$

$$I_{GABA}(t) = g_{GABA}(V(t) - V_I) \sum_{j=1}^N w_j s_j^{GABA}(t) \quad (\text{Eq. 5})$$

$$I_{NMDA}(t) = \frac{g_{NMDA}(V(t) - V_E)}{1 + [\text{Mg}^{2+}] \exp(-\frac{0.062V(t)}{3.57})} \sum_{j=1}^N w_j s_j^{NMDA}(t) \quad (\text{Eq. 6})$$

where the reversal potentials are  $V_E=0$  mV,  $V_I = V_{rest}$ , and each group of inhibitory interneurons has its own  $V_{rest}$ . The  $g$  terms represent the conductances of the specific receptor types. The weights  $w_j$  represent the strength of each synapse received by the neuron. The sum runs over all presynaptic neurons  $j$  projecting to the neuron under consideration. NMDAR currents have a voltage dependence controlled by extracellular magnesium concentration<sup>40</sup>,  $[\text{Mg}^{2+}]=1$  mM. The  $s$  terms represent the gating variables, or fraction of open channels and their behaviour is governed by the following equations.

First, the AMPAR channels are described by

$$\frac{ds_j^{AMPA}(t)}{dt} = \frac{-s_j^{AMPA}(t)}{\tau_{AMPA}} + \sum_k \delta(t - t_j^k) \quad (\text{Eq. 7})$$

where the time constant of the AMPA currents is  $\tau_{AMPA} = 2$  ms, and the sum over  $k$  represents the contribution of all spikes (indicated by delta,  $\delta$ ) emitted by presynaptic neuron  $j$ . In the case of external AMPA currents (Eq. 3), the spikes are emitted accordingly to a Poisson process with rate  $\nu_{bkgnd}$ . Each group of cells in each layer is receiving a different Poisson rate of background noise (see Table S9). The gating of single NMDAR channels is described by

$$\frac{ds_j^{NMDA}(t)}{dt} = \frac{-s_j^{NMDA}(t)}{\tau_{NMDA,decay}} + \alpha x_j(t)(1 - s_j^{NMDA}(t)) \quad (\text{Eq. 8})$$

$$\frac{dx_j(t)}{dt} = \frac{-x_j(t)}{\tau_{NMDA,rise}} + \sum_k \delta(t - t_j^k) \quad (\text{Eq. 9})$$

where the decay and rise time constants of NMDAR current are 80 ms and 2 ms respectively, and the constant  $\alpha = 0.5 \text{ ms}^{-1}$ . The GABA<sub>A</sub> receptor synaptic variable is described by

$$\frac{ds_j^{GABA}(t)}{dt} = \frac{-s_j^{GABA}(t)}{\tau_{GABA}} + \sum_k \delta(t - t_j^k) \quad (\text{Eq. 10})$$

where the time constant of GABA<sub>A</sub> receptor current is 5 ms.

### Parameters of the model

As previously mentioned, each type of cell in each layer is characterized by its own set of parameters: a resting potential  $V_{rest}$ , a firing threshold  $V_{th}$ , a membrane capacitance  $C_m$ , a membrane leak conductance  $g_L$  and a refractory period  $\tau_{ref}$ . These data are taken from the Allen institute database (<https://portal.brain-map.org/explore/models/mv1-all-layers>). In particular, for each type of cell in each layer the Allen database proposes different subsets of cells (e.g. two different PV subtypes in L4), each with its own set of parameters. To

simplify the model, for each layer we only used one set of parameters for each cell type, choosing the set of parameters of the most prevalent subset of cells. The parameters  $C_m$ ,  $g_L$ ,  $\tau_{ref}$ ,  $V_{rest}$ ,  $V_{th}$  used for each cell type in each layer are reported in Tables S4-S8.

#### Details on the background noise

All neurons received background noise, representing the influence of the 'rest of the brain' on the modeled area, as shown in Figure 1. Excitatory postsynaptic currents (EPSCs) due to background noise are exclusively mediated in the model by AMPA receptors, denoted as  $I_{ext,AMPA}(t)$  (Eq. 3). The levels of background noise that each group of cells received can be found in Supplementary Table 9. The firing rate  $v_{bkgnd}$  of the background Poissonian pulse generators connected to each group differed among them.

Each neuron in every group is connected to its own background Poisson generator. Thus, even though the rates  $v_{bkgnd}$  of the Poisson generators are the same for all neurons within the same group, each specific cell receives its own different pulse train.

#### Details on the weights

The weight of each synapse  $w_j$  from neurons of group A to neurons in group B is chosen to be equal to

$$w_j = G * \frac{\hat{s}}{N_{send} p} \quad (\text{Eq. 11})$$

where  $G=5$  is the global coupling factor,  $\hat{s}$  is the overall strength between the two connected groups of cells,  $N_{send}$  is the number of neurons in the sending population A, and  $p$  the probability of connection between the neurons of the two groups (A and B) taken from the experimental probability matrix  $P$ . For each pair of connected groups,  $\hat{s}$  is taken from the experimental synaptic connectivity matrix  $S$ , defined by the  $16 \times 16 + 16 \times 2 = 288$  synaptic strengths between the 17 considered cell types (4 groups in each of the 4 layers + 1 group in layer 1). Matrices  $S$  and  $P$  can be found at <https://portal.brain-map.org/explore/models/mv1-all-layers>. The normalization in Eq. 11 above guarantees that the dynamics and equilibrium points of the system scale properly with the size of the network (Fig. S2).

The spikes generated by an excitatory neuron can target AMPA or/and NMDA receptors of the postsynaptic receiving neuron. The AMPA and NMDA receptors are chosen to be in a 0.8 and 0.2 ratio respectively. Thus, the probability of connection  $p$  between the neurons of the two groups (A and B) is multiplied by 0.2 for NMDA receptors and 0.8 for AMPA receptors. For example suppose excitatory neurons in group A are connected to neurons in group B with a probability  $p$  (taken from the matrix P). Then the excitatory connections targeting the AMPA receptors of group B will be chosen with  $p_{AMPA} = p * 0.8$  and those targeting NMDA receptors will be chosen with  $p_{NMDA} = p * 0.2$ .

### Synaptic plasticity rule

After having performed simulations with fixed weights, we explored the consequences of allowing synaptic plasticity in the model. To include plasticity we used the STDP learning rule<sup>50</sup>, given by

$$\Delta w_{ji} = \sum_f \sum_n F(t_i^n - t_j^f) \quad (\text{Eq. 12})$$

where  $n$  is the index for the spike times of postsynaptic neuron  $j$ , and  $f$  the index for the spike times of presynaptic neuron  $j$ . The weight change of a synapse depends on the relative timing between pre- and postsynaptic spikes. The function used to account for this change is the following:

$$F(x) = \begin{cases} A_+ \exp\left(-\frac{x}{\tau_+}\right), & x > 0 \\ -A_- \exp\left(\frac{x}{\tau_-}\right), & x < 0 \end{cases} \quad (\text{Eq. 13})$$

where  $x$  is the difference between the spike time of the postsynaptic neuron minus the spike time of the presynaptic neuron, and  $\tau_+$  and  $\tau_-$  are time constants, both with the same value of 20 ms. Likewise, we set the parameters  $A_+=0.02$  and  $A_-=0.021$ .

The values used to initialize the weights are defined using the  $S$  matrix (Eq. 11).

Only excitatory-to-excitatory weights are allowed to change; inhibitory connections are kept fixed during the simulation.

All differential equations were numerically solved using Euler's method, using a time step of 0.1 ms.

**Acknowledgments:**

This work was done with the support of EBRAINS and HBP computing services. We thank Matthias Brucklacher, Kwangjun Lee and Parva Alavian for constructive discussions, and Hans Ekkehard Plessner, Sacha van Albada, Walter Senn and Sander Bohte for their useful feedback on early iterations of the work.

**Funding:** This project has received funding from the European Union's Horizon 2020 Framework Programme for Research and Innovation under the Specific Grant Agreement No. 945539 (Human Brain Project SGA3; to CMAP, JFM), the NWA-ORC grant "Acting under uncertainty" (JFM, CMAP), and a UvA/ABC Project Grant (JFM).

**Author contributions:** JFM and CP conceived and designed the study; GM performed the research; GM and JFM analyzed the results, GM, CP and JFM wrote the manuscript.

**Competing interests:** Authors declare not competing interests.

**Data and materials availability:** All information needed to reproduce the results of this manuscript are in the main text and Materials and Methods section, and the code used will be made available upon publication of this work.

## References

1. Bosman, C. A., Lansink, C. S. & Pennartz, C. M. A. Functions of gamma-band synchronization in cognition: from single circuits to functional diversity across cortical and subcortical systems. *Eur. J. Neurosci.* **39**, 1982–1999 (2014).
2. Bastos, A. M. *et al.* Visual Areas Exert Feedforward and Feedback Influences through Distinct Frequency Channels. *Neuron* **85**, 390–401 (2015).
3. Vinck, M. & Bosman, C. A. More Gamma More Predictions: Gamma-Synchronization as a Key Mechanism for Efficient Integration of Classical Receptive Field Inputs with Surround Predictions. *Front. Syst. Neurosci.* **10**, (2016).
4. Wang, X.-J. Neurophysiological and Computational Principles of Cortical Rhythms in Cognition. *Physiol. Rev.* **90**, 1195–1268 (2010).
5. Papadopoulos, L., Battaglia, D. & Bassett, D. S. Controlling collective dynamical states of mesoscale brain networks with local perturbations. Preprint at <https://doi.org/10.48550/arXiv.2208.12231> (2022).
6. Tiesinga, P. & Sejnowski, T. J. Cortical Enlightenment: Are Attentional Gamma Oscillations Driven by ING or PING? *Neuron* **63**, 727–732 (2009).
7. Brunel, N. & Wang, X.-J. What Determines the Frequency of Fast Network Oscillations With Irregular Neural Discharges? I. Synaptic Dynamics and Excitation-Inhibition Balance. *J. Neurophysiol.* **90**, 415–430 (2003).
8. Wilson, H. R. & Cowan, J. D. Excitatory and Inhibitory Interactions in Localized Populations of Model Neurons. *Biophys. J.* **12**, 1–24 (1972).
9. Brunel, N. Dynamics of Sparsely Connected Networks of Excitatory and Inhibitory Spiking Neurons. *J. Comput. Neurosci.* **8**, 183–208 (2000).

10. Rudy, B., Fishell, G., Lee, S. & Hjerling-Leffler, J. Three groups of interneurons account for nearly 100% of neocortical GABAergic neurons. *Dev. Neurobiol.* **71**, 45–61 (2011).
11. Tremblay, R., Lee, S. & Rudy, B. GABAergic Interneurons in the Neocortex: From Cellular Properties to Circuits. *Neuron* **91**, 260–292 (2016).
12. Cardin, J. A. *et al.* Driving fast-spiking cells induces gamma rhythm and controls sensory responses. *Nature* **459**, 663–667 (2009).
13. Antonoudiou, P., Tan, Y. L., Kontou, G., Upton, A. L. & Mann, E. O. Parvalbumin and Somatostatin Interneurons Contribute to the Generation of Hippocampal Gamma Oscillations. *J. Neurosci.* **40**, 7668–7687 (2020).
14. Onorato, I. *et al.* Distinct roles of PV and Sst interneurons in visually-induced gamma oscillations. 2023.04.08.535291 Preprint at <https://doi.org/10.1101/2023.04.08.535291> (2023).
15. Litwin-Kumar, A., Rosenbaum, R. & Doiron, B. Inhibitory stabilization and visual coding in cortical circuits with multiple interneuron subtypes. *J. Neurophysiol.* **115**, 1399–1409 (2016).
16. Wood, K. C., Blackwell, J. M. & Geffen, M. N. Cortical inhibitory interneurons control sensory processing. *Curr. Opin. Neurobiol.* **46**, 200–207 (2017).
17. Fries, P. A mechanism for cognitive dynamics: neuronal communication through neuronal coherence. *Trends Cogn. Sci.* **9**, 474–480 (2005).
18. Vinck, M. *et al.* Cell-Type and State-Dependent Synchronization among Rodent Somatosensory, Visual, Perirhinal Cortex, and Hippocampus CA1. *Front. Syst. Neurosci.* **9**, (2016).

19. Battaglia, D. & Hansel, D. Synchronous Chaos and Broad Band Gamma Rhythm in a Minimal Multi-Layer Model of Primary Visual Cortex. *PLOS Comput. Biol.* **7**, e1002176 (2011).
20. Mejias, J. F., Murray, J. D., Kennedy, H. & Wang, X.-J. Feedforward and feedback frequency-dependent interactions in a large-scale laminar network of the primate cortex. *Sci. Adv.* **2**, e1601335 (2016).
21. Dowdall, J. R. & Vinck, M. Coherence fails to reliably capture inter-areal interactions in bidirectional neural systems with transmission delays. *NeuroImage* **271**, 119998 (2023).
22. Schneider, M. *et al.* A mechanism for inter-areal coherence through communication based on connectivity and oscillatory power. *Neuron* **109**, 4050-4067.e12 (2021).
23. Spaak, E., Bonnefond, M., Maier, A., Leopold, D. A. & Jensen, O. Layer-Specific Entrainment of Gamma-Band Neural Activity by the Alpha Rhythm in Monkey Visual Cortex. *Curr. Biol.* **22**, 2313–2318 (2012).
24. Jensen, O. & Mazaheri, A. Shaping Functional Architecture by Oscillatory Alpha Activity: Gating by Inhibition. *Front. Hum. Neurosci.* **4**, (2010).
25. Binzegger, T., Douglas, R. J. & Martin, K. A. C. A Quantitative Map of the Circuit of Cat Primary Visual Cortex. *J. Neurosci.* **24**, 8441–8453 (2004).
26. Thomson, A. M., West, D. C., Wang, Y. & Bannister, A. P. Synaptic Connections and Small Circuits Involving Excitatory and Inhibitory Neurons in Layers 2–5 of Adult Rat and Cat Neocortex: Triple Intracellular Recordings and Biocytin Labelling In Vitro. *Cereb. Cortex* **12**, 936–953 (2002).
27. Potjans, T. C. & Diesmann, M. The Cell-Type Specific Cortical Microcircuit: Relating Structure and Activity in a Full-Scale Spiking Network Model. *Cereb. Cortex* **24**, 785–806 (2014).

28. Billeh, Y. N. *et al.* Systematic Integration of Structural and Functional Data into Multi-scale Models of Mouse Primary Visual Cortex. *Neuron* **106**, 388-403.e18 (2020).
29. Albada, S. J. van, Helias, M. & Diesmann, M. Scalability of Asynchronous Networks Is Limited by One-to-One Mapping between Effective Connectivity and Correlations. *PLOS Comput. Biol.* **11**, e1004490 (2015).
30. van Kerkoerle, T. *et al.* Alpha and gamma oscillations characterize feedback and feedforward processing in monkey visual cortex. *Proc. Natl. Acad. Sci.* **111**, 14332–14341 (2014).
31. Renart, A. *et al.* The Asynchronous State in Cortical Circuits. *Science* **327**, 587–590 (2010).
32. Golomb, D. Neuronal synchrony measures. *Scholarpedia* **2**, 1347 (2007).
33. Douglas, R. J. & Martin, K. A. C. Neuronal Circuits of the Neocortex. *Annu. Rev. Neurosci.* **27**, 419–451 (2004).
34. Gilbert, C. D. Microcircuitry of the Visual Cortex. *Annu. Rev. Neurosci.* **6**, 217–247 (1983).
35. Olsen, S. R., Bortone, D. S., Adesnik, H. & Scanziani, M. Gain control by layer six in cortical circuits of vision. *Nature* **483**, 47–52 (2012).
36. Henrie, J. A. & Shapley, R. LFP Power Spectra in V1 Cortex: The Graded Effect of Stimulus Contrast. *J. Neurophysiol.* **94**, 479–490 (2005).
37. Ray, S. & Maunsell, J. H. R. Differences in Gamma Frequencies across Visual Cortex Restrict Their Possible Use in Computation. *Neuron* **67**, 885–896 (2010).
38. Jia, X., Xing, D. & Kohn, A. No Consistent Relationship between Gamma Power and Peak Frequency in Macaque Primary Visual Cortex. *J. Neurosci.* **33**, 17–25 (2013).

39. Perrenoud, Q., Pennartz, C. M. A. & Gentet, L. J. Membrane Potential Dynamics of Spontaneous and Visually Evoked Gamma Activity in V1 of Awake Mice. *PLOS Biol.* **14**, e1002383 (2016).
40. Wang, X.-J. Synaptic Basis of Cortical Persistent Activity: the Importance of NMDA Receptors to Working Memory. *J. Neurosci.* **19**, 9587–9603 (1999).
41. Bernander, O., Douglas, R. J., Martin, K. A. & Koch, C. Synaptic background activity influences spatiotemporal integration in single pyramidal cells. *Proc. Natl. Acad. Sci.* **88**, 11569–11573 (1991).
42. Huang, C., Zeldenrust, F. & Celikel, T. Cortical Representation of Touch in Silico. *Neuroinformatics* **20**, 1013–1039 (2022).
43. Mejias, J. F. & Longtin, A. Optimal Heterogeneity for Coding in Spiking Neural Networks. *Phys. Rev. Lett.* **108**, 228102 (2012).
44. Mejias, J. F. & Longtin, A. Differential effects of excitatory and inhibitory heterogeneity on the gain and asynchronous state of sparse cortical networks. *Front. Comput. Neurosci.* **8**, (2014).
45. Miller, E. K., Lundqvist, M. & Bastos, A. M. Working Memory 2.0. *Neuron* **100**, 463–475 (2018).
46. Jadi, M. P., Behrens, M. M. & Sejnowski, T. J. Abnormal Gamma Oscillations in N-Methyl-D-Aspartate Receptor Hypofunction Models of Schizophrenia. *Biol. Psychiatry* **79**, 716–726 (2016).
47. Kyuhou, S. & Gemba, H. Fast cortical oscillation after thalamic degeneration: Pivotal role of NMDA receptor. *Biochem. Biophys. Res. Commun.* **356**, 187–192 (2007).
48. Mejias, J. F. & Wang, X.-J. Mechanisms of distributed working memory in a large-scale network of macaque neocortex. *eLife* **11**, e72136 (2022).

49. Feng, M., Bandyopadhyay, A. & Mejias, J. F. Emergence of distributed working memory in a human brain network model. 2023.01.26.525779 Preprint at <https://doi.org/10.1101/2023.01.26.525779> (2023).
50. Gerstner, W., Kempter, R., van Hemmen, J. L. & Wagner, H. A neuronal learning rule for sub-millisecond temporal coding. *Nature* **383**, 76–78 (1996).

**Supplementary figures:**

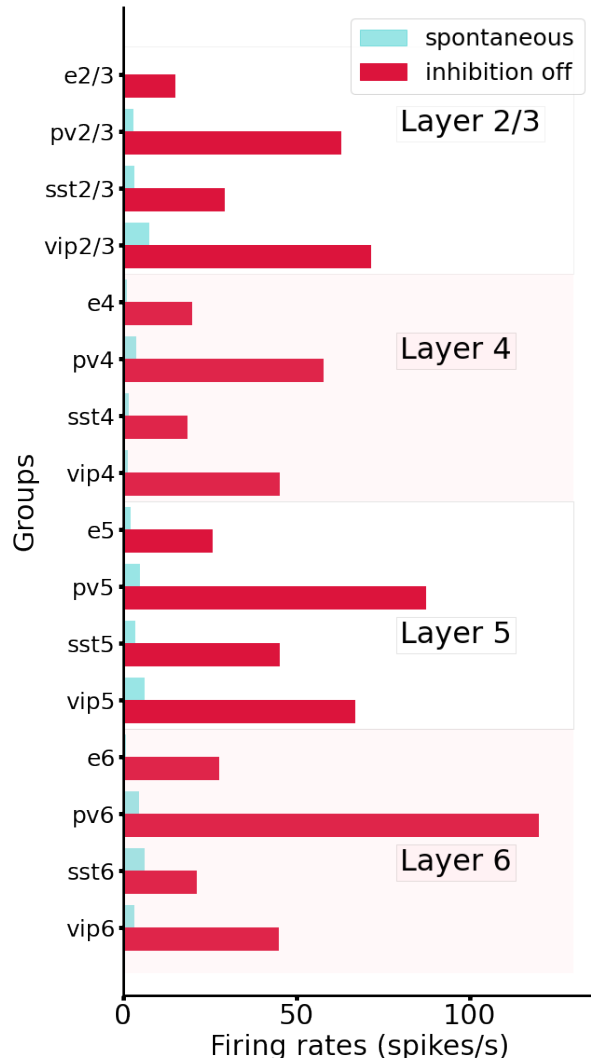


*Figure S1: Comparison between spontaneous activity in normal conditions (control, blue) vs. the condition of disabling the output from all inhibitory neurons (while maintaining their capacity to spike). All groups substantially elevated their firing rates, particularly those in deep layers.*

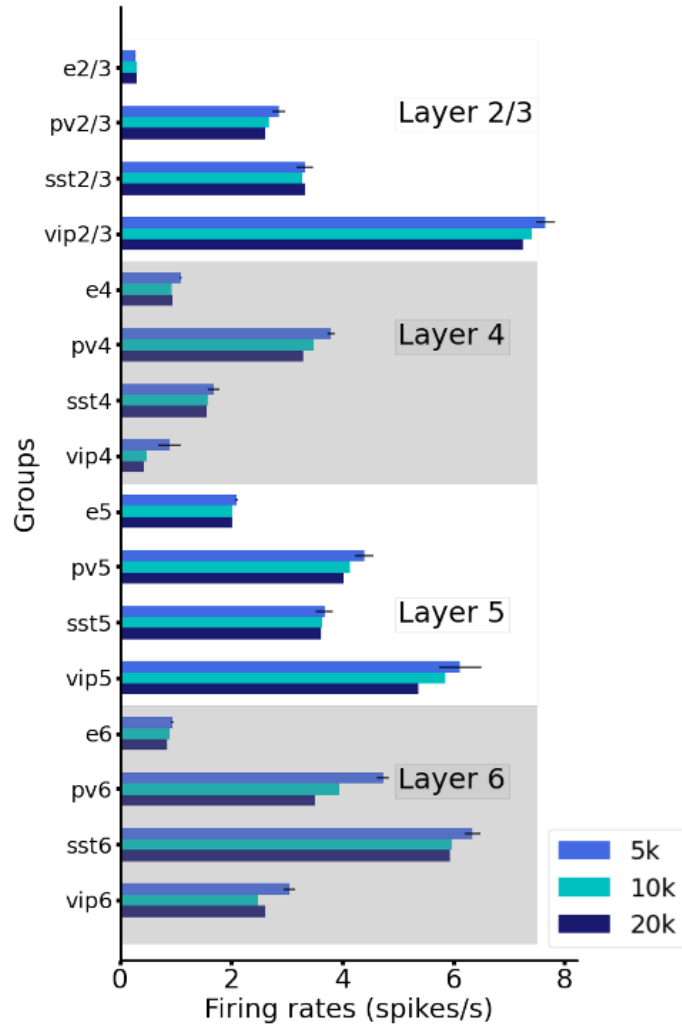


*Figure S2: Mean firing rates of all groups for networks of different sizes. We show that, with proper scaling of the weights (see Methods), results for 5000 neurons, 10000 neurons and 20000 neurons lead to the very similar results.*

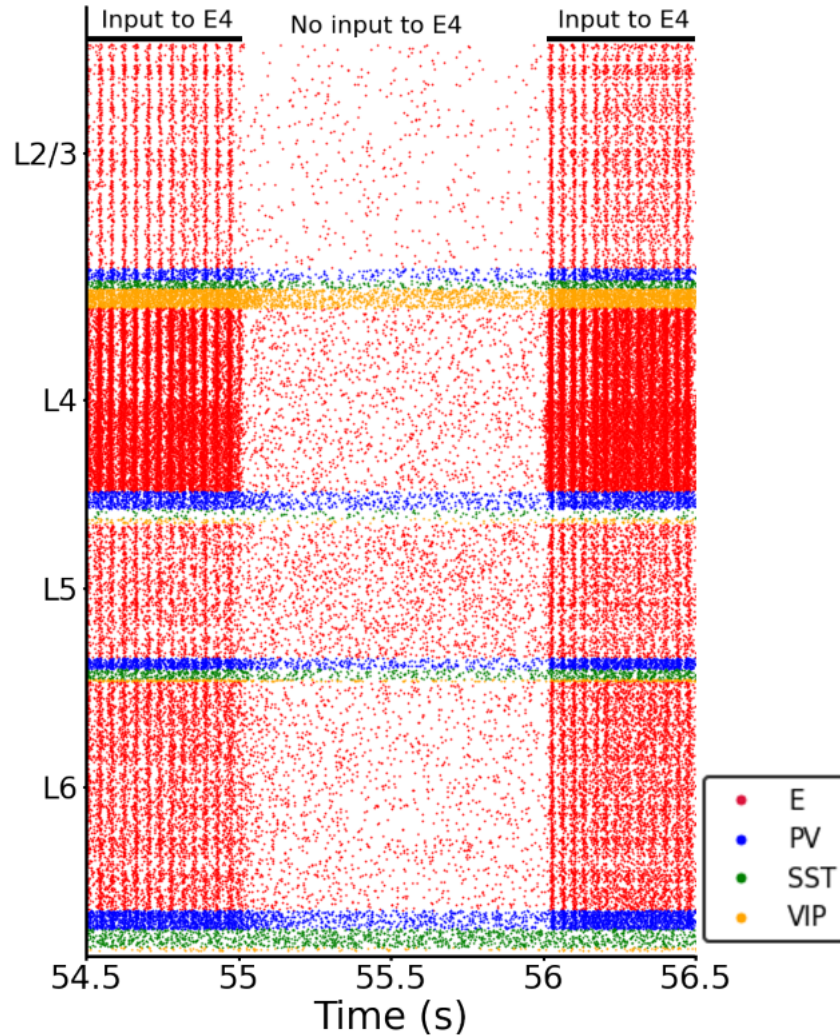


*Figure S3: Raster plot showing the relations between input to layer 4 and oscillations. STDP plasticity was present from the start of the simulation until 55 s. When the input was switched off at t=55 s, the oscillations (frequency: 26 Hz) disappeared; vice versa for switching the input back on. All hyperparameters of this simulations are listed in Tables S3-S9.*

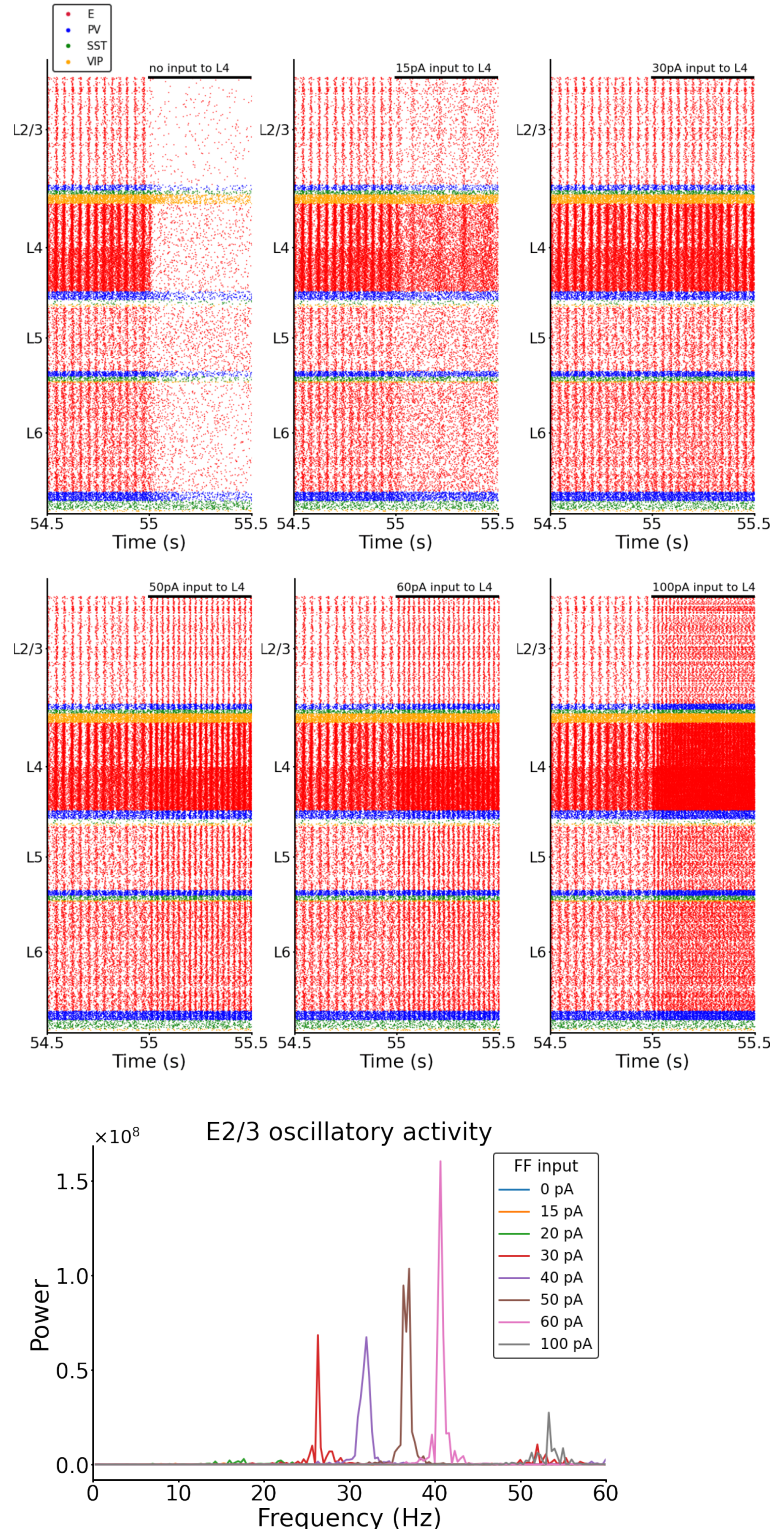


**Figure S4: Modulation of oscillations by feedforward input strength.** Top: Raster plots of a subset of the conditions shown in Fig.5A (varying input strength to excitatory cells in layer 4: no input, 15 pA, 30 pA, 50 pA, 60 pA, 100 pA). Applying more input to layer 4 causes faster oscillations. When no input to layer 4 is present the oscillations disappear. Bottom: Power spectrum of the frequency of excitatory Layer 2/3 neuron firing with varying feedforward input to layer 4 (each color trace represents a different amount of feedforward input to layer 4). The peak amplitudes (max power) and the corresponding frequency are also shown in Fig. 5B and 5C.

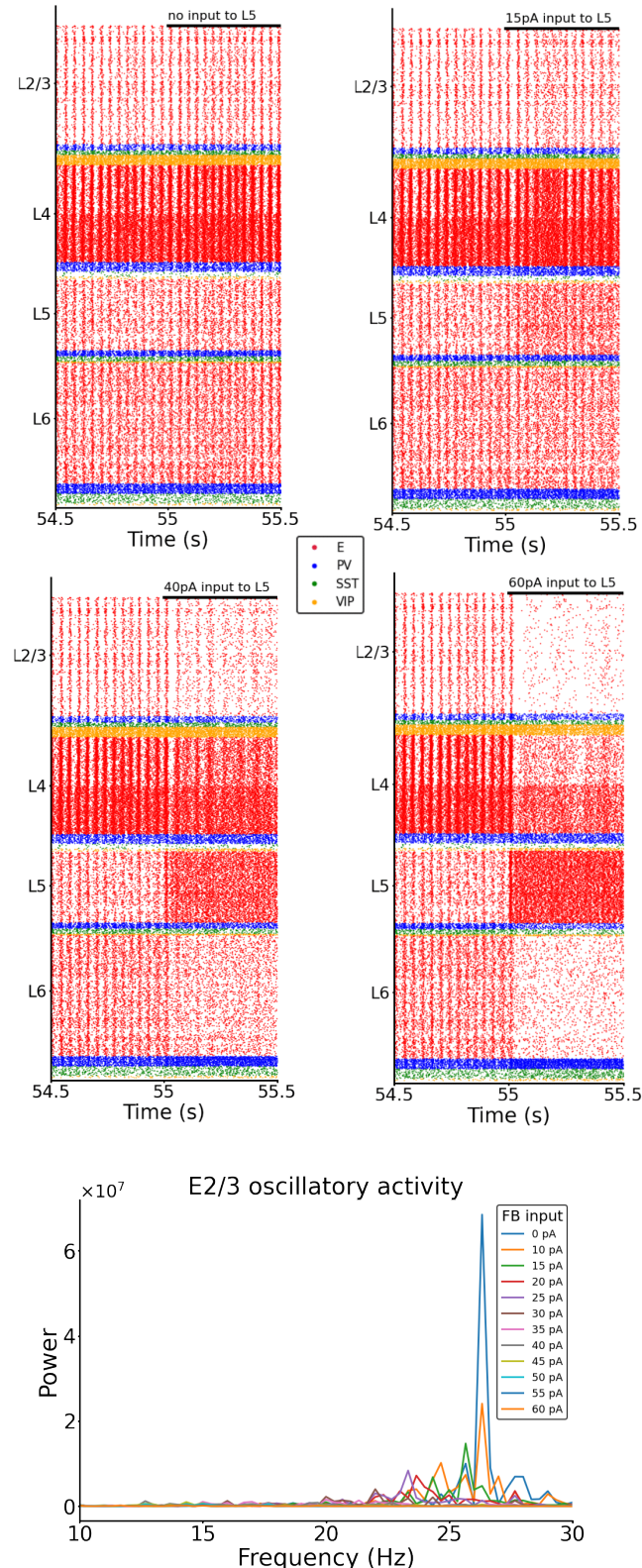


*Figure S5: Modulation of oscillations by feedback (FB) input strength. Top: Raster plots of a subset of the conditions shown in Fig. 5D (varying input strength to excitatory cells in layer 5: no feedback input, 15 pA, 40 pA, 60 pA). The more input is applied to layer 5 (while keeping a constant input of 30 pA to layer 4) the more the oscillations slow down and decrease in power. Bottom: Power spectrum of the frequency of excitatory layer 2/3 neuron firing with varying feedback input (each color trace represents a different amount of feedback inout to layer 5). The peak amplitudes (max power) and the corresponding frequency are also shown in Fig. 5E and 5F.*

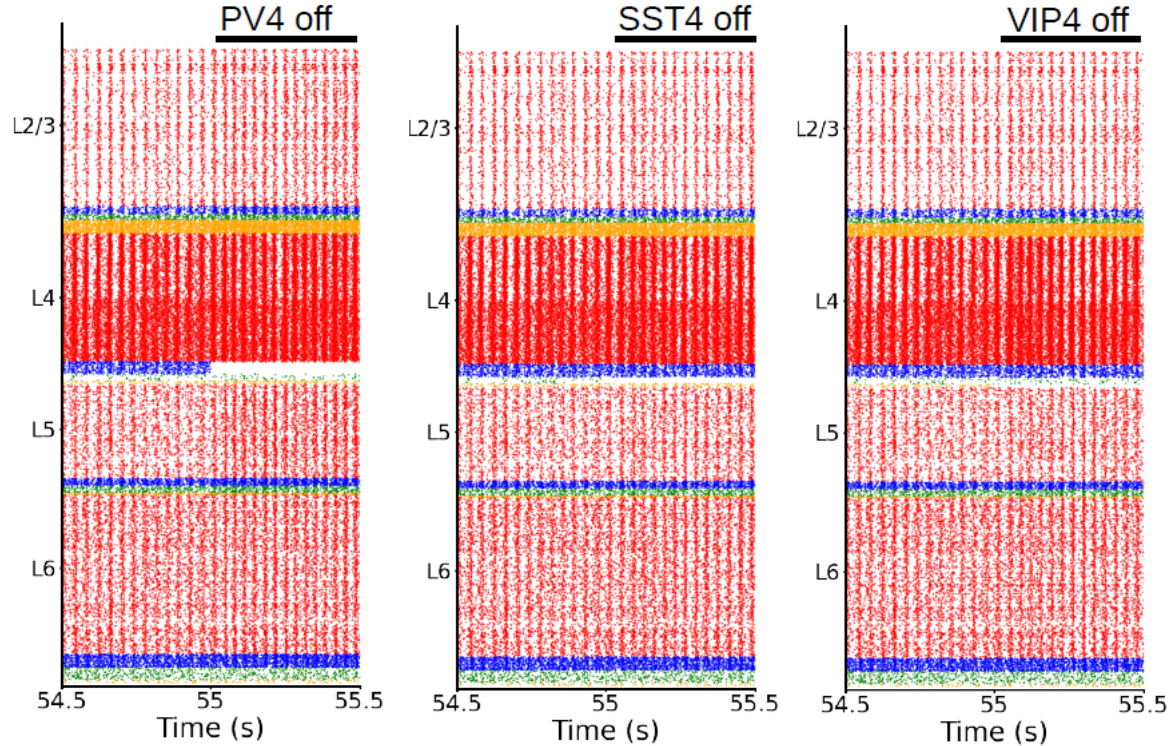


*Figure S6: Raster plots of the whole column model for inactivating different cell groups in layer 4. Each group is inactivated (one at a time) at 55 s to visualize the effects on neural dynamics. From left to right: inactivation of PV neuron in layer 4, SST neurons in layer 4, VIP neurons in layer 4. Removing one group of inhibitory neurons at a time has only a minor effect on the oscillations: a slight increase of the oscillations speed. A bigger effect in increasing the speed of oscillations is however shown in the case of silencing PV cells (leftmost raster plot).*

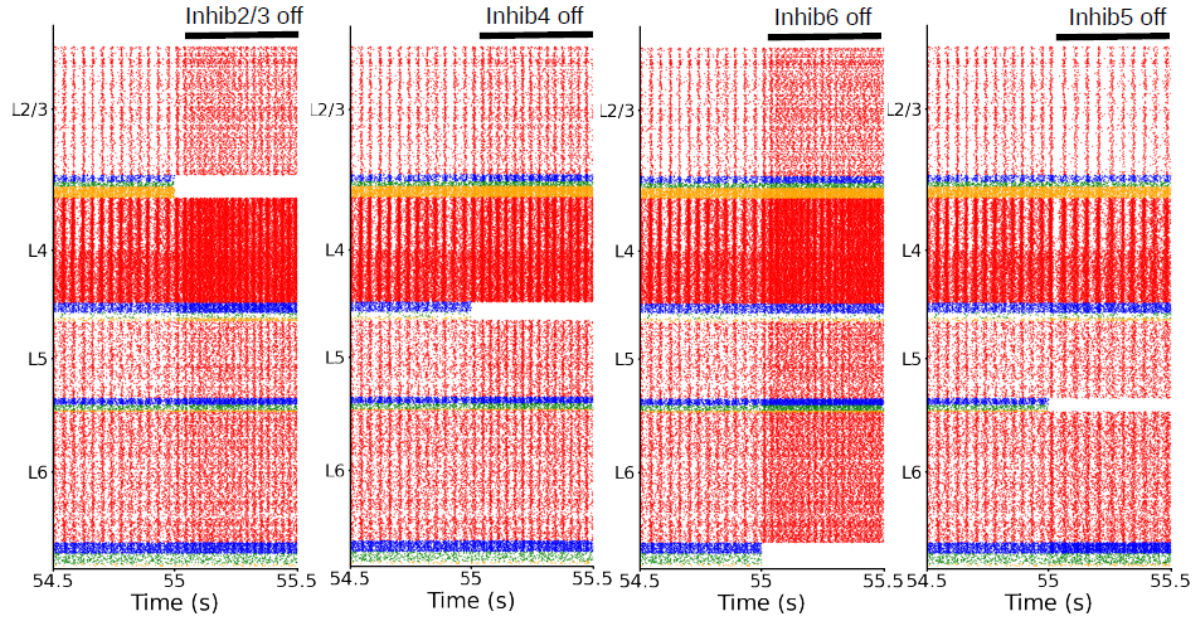


*Figure S7: Raster plots of the whole column model for different inactivation conditions (layer analysis). All inhibitory cells in a layer are inactivated at 55 s, to visualize the effects on neural dynamics. From left to right: inactivation of all inhibitory neurons in layer 2/3, layer 4, layer 6, layer 5. All inhibitory neuron types in each layer contribute to oscillations, removing them one layer at a time shows their effect (increase of oscillation frequency). The inactivation of the inhibitory neurons in Layer 2/3 show the biggest effect. Layer 5 is the only exception: here the oscillations decrease in frequency and power.*

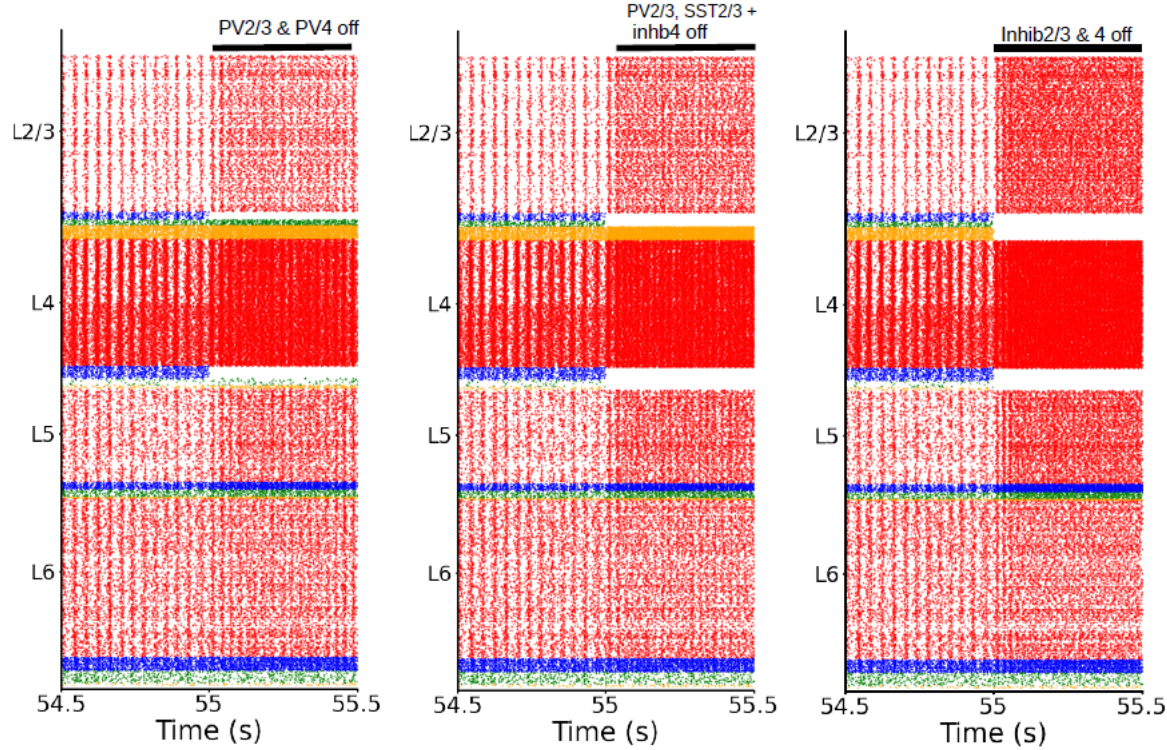


*Figure S8: Raster plots of the whole column model for different inactivation conditions. Each combination of groups is inactivated at 55 s. From left to right: inactivation of PV cells in layer 2/3 and PV cells in layer 4; inactivation of PV and SST cells in layer 2/3; and all inhibitory cells in layer 4, inactivation of all inhibitory neurons in layer 2/3 and 4. Removing more and more groups (from left to right) causes a significant increase in oscillation frequency.*

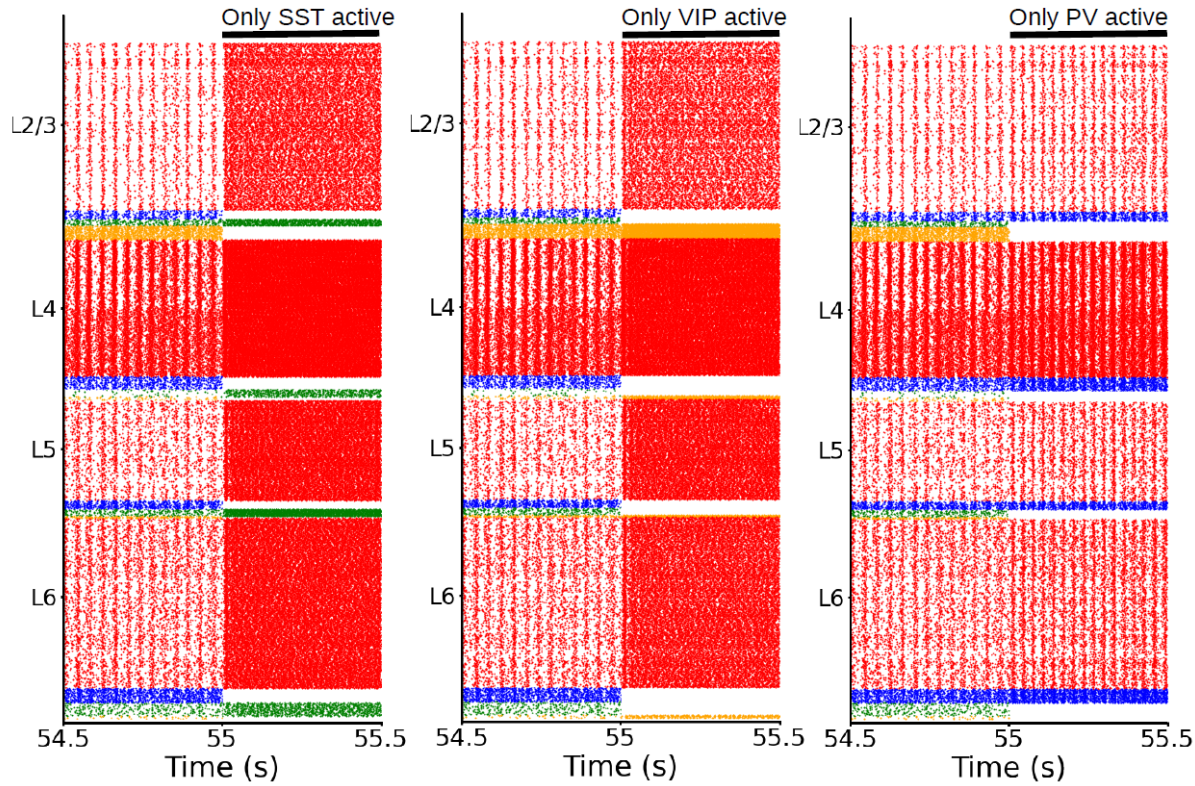


*Figure S9: Raster plots of the whole column model for different inactivation conditions. Each cell type across all layers is inactivated at 55 s. These are experiments where we are leaving active only one type of inhibitory neurons in the entire column (next to pyramidal cells). From left to right: only SST active, only VIP active, only PV active. This shows that – together with pyramidal cells – PV cells alone are able to maintain oscillations around the same frequency (26 Hz). Only a slight increase is visible, the same is not true for SST or VIP. When only them are active the oscillations are drastically affected (first two raster plots).*

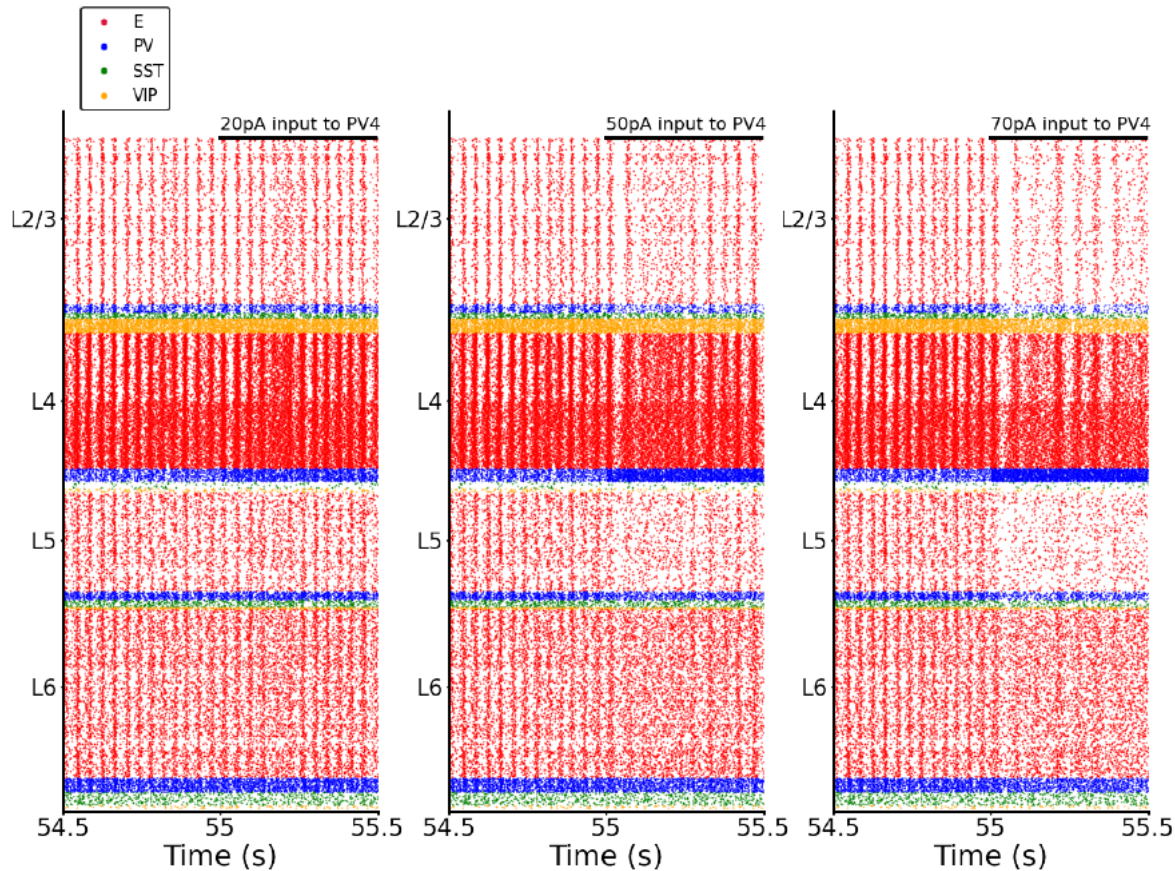


*Figure S10: Raster plots of the whole column model for different input strengths applied to PV neurons in layer 4. The input is given at 55 s. From left to right: 20 pA of input to PV in layer 4, 50 pA of input to PV in layer 4, 70 pA of input to PV in layer 4. Injecting more input into PV cells shows that they are able to modulate the frequency of the oscillations. The more input to layer 4 PV the more the oscillation frequency decreases. In the first two raster plots, a blurring of the oscillations can be observed after 55 seconds. The excitatory neurons are receiving increased inhibition from the PV cells (which are also receiving external input). As a result, the synchrony of their firing, which generates the oscillations, is partially lost, leading to this observable effect.*

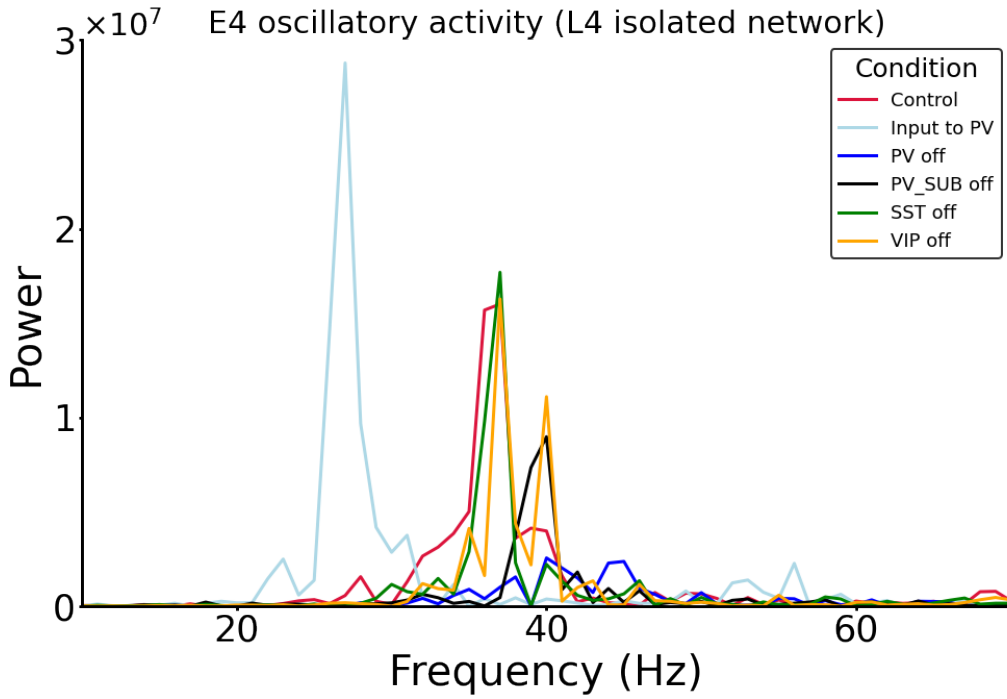


*Figure S11: Power spectrum of the frequency of excitatory neuron firing in layer 4 for different inactivation conditions for the isolated network of layer 4 (schematics in Fig. 6C left). Each color trace represents a different condition, in the legend the name of the group (PV, SST, VIP) represents the inhibited group. Here we can appreciate the shift in the power peak depending on the analyzed condition: when PV cells are inactivated the frequency with max power (peak in the plot) is shifted to the right (blue), indicating an increase in speed of the oscillations. In contrast, when PV cells are stimulated by an external input they modulate the frequency of the oscillations which shows a significant decrease (lightblue trace: Input to PV). This result is consistent with the full-model scenario shown in S10. A total inhibition of SST cells or VIP cells is not significantly affecting the oscillations (green and yellow trace). The maxima of oscillatory power at 37 Hz for the different conditions were also shown in Fig. 6C (left) as well as the frequency where maximal power was reached (right in Fig. 6C).*

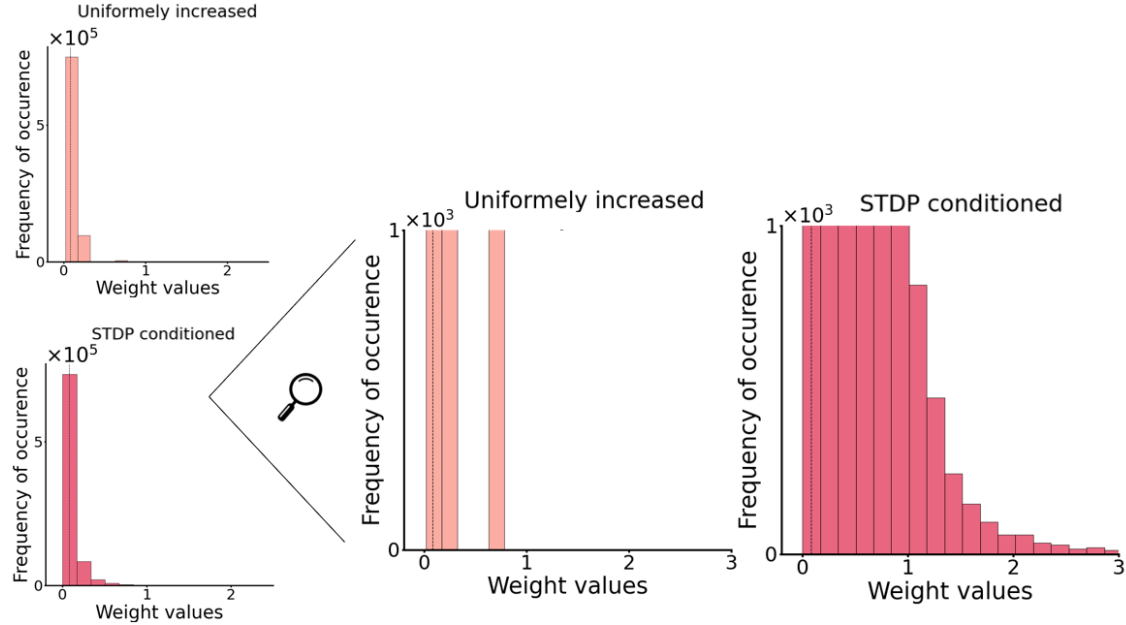


*Figure S12: Weights distribution for the trained network and uniformly increased network (see Fig. 7). Left: distribution of weights for the two networks. Right: zoom in by cutting the threshold on the y-axis at  $10^3$  to better visualize the differences between the distributions. Even if the average of all connection strengths of the STDP conditioned and Uniformly increased network are the same (mean=0.081) a closer look at the left panel shows that the distributions are different. In the Uniformly increased network, there are few connections (less than 600 out of the total of 800k) that have a high value ( $>1.5$ ). Those strong connections are absent in the Uniformly increased network. The reason that the means of the two distributions are so similar, is that in the STDP contiditioned network the vast majority of connections are very small  $\sim 0$ , which collectively compensates for the small subset of strong connections. In the Uniformly increased network those strong connections are absent, in conjunction with the absence oscillations.*

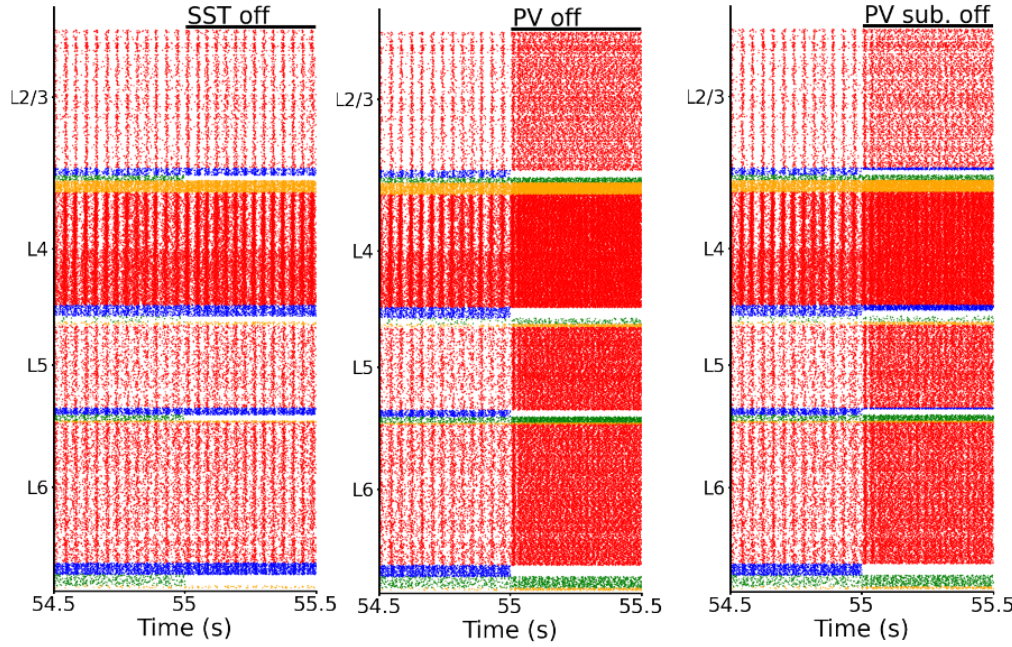
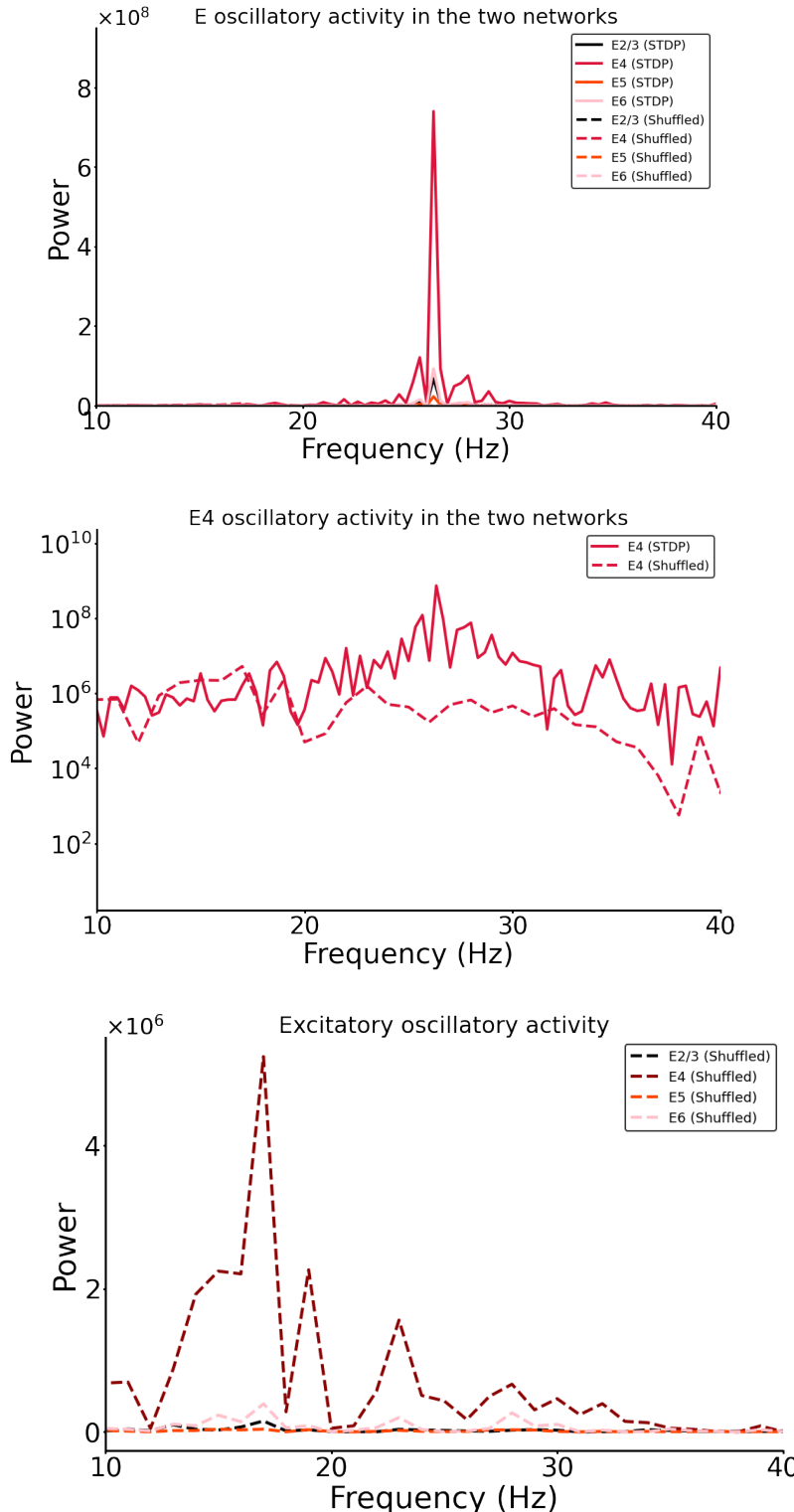


*Figure S13: Raster plots of the entire column model under different inactivation conditions. Each cell type across all layers is inactivated at 55 seconds. The first two raster plots are also shown in 6B. From left to right: the effect of silencing all SST cells, all PV cells, and a subset of PV cells. To test whether the impact of PV cells was not solely due to the higher number of PV cells compared to SST cells, we inactivated a subpopulation of PV cells (PV-sub), equal in size to the number of SST neurons in each layer. The effects on the oscillations, in this case, were significantly stronger than the inactivation of the SST population, thereby proving the stronger role of PV cells. The prominent role of PV cells appeared to be related, not solely to their higher number, but rather to the synaptic connections from PV to pyramidal neurons, which are stronger than the projections from SST to pyramidal neurons.*



Network type	Frequency	E2/3	E4	E5	E6
STDP conditioned	26 Hz	$6.8 * 10^7$	$7.4 * 10^8$	$2.3 * 10^7$	$9.3 * 10^7$
Shuffled	26 Hz	$7.7 * 10^3$	$7.8 * 10^2$	$7.2 * 10^2$	$4.7 * 10^3$
Shuffled	17 Hz	$1.5 * 10^5$	$5.2 * 10^6$	$3.7 * 10^4$	$3.9 * 10^5$

*Figure S14: Top: Power spectrum of the frequency of excitatory neuron firing rates in all layers of two distinct networks (STDP conditioned and Shuffled networks). As shown in Figure 7A, in the network with shuffled weights, the oscillatory activity disappears. The peaks at 26 Hz in the Shuffled network are no longer visible. Middle: Power spectrum of the frequency of excitatory neuron firing rates in layer 4 of the two distinct networks (STDP conditioned and Shuffled networks). A logarithmic scale is used to better appreciate the power drop. Bottom: Power spectrum of the frequency of excitatory neuron firing rates in all layers for the Shuffled network. The maximum peak is at 17 Hz; the power at 26 Hz is now irrelevant compared to the STDP conditioned network. Table: Values of the power of the frequency of excitatory neuron firing rates in all layers of two distinct networks (STDP conditioned and Shuffled networks) at 26 Hz (frequency with maximum power for the STDP conditioned network) and 17 Hz (frequency with maximum power for the Shuffled network). In the Shuffled network, the power at 26 Hz drastically drops (e.g., value drops from  $10^7$  to  $10^3$  for excitatory neurons in Layer 2/3).*

## Tables

*Table 1: Number of neurons in each layer.  $N_{tot}$  is the total number of cells in the column and can be defined arbitrarily for a simulation. The number of cells in each layer will scale accordingly. We used  $N_{tot}=5000$  for all main simulations. In S2 we showed the results for  $N_{tot}=10000$  and  $N_{tot}=20000$ .*

	Number of neurons
L1	0.0192574218*N <sub>tot</sub>
L2/3	0.291088453*N <sub>tot</sub>
L4	0.237625904*N <sub>tot</sub>
L5	0.17425693*N <sub>tot</sub>
L6	0.297031276*N <sub>tot</sub>

*Table 2: Percentage of inhibitory neurons as a fraction of the total number of inhibitory cells in each layer. In each layer, the inhibitory cells represent 15% of the total number of neurons for that layer.*

Percentage (%)	PV	SST	VIP
L2/3	0.295918	0.214286	0.489796
L4	0.552381	0.295238	0.152381
L5	0.485714	0.428571	0.085714
L6	0.458333	0.458333	0.083333

*Table 3: Cell counts in the network for  $N_{tot} = 5000$ .*

Number of neurons	E	PV	SST	VIP
L1				96
L2/3	1236	65	47	107
L4	1010	98	53	27
L5	741	63	56	11
L6	1263	102	102	19

*Table 4: Membrane capacitance for each group of cells. The values are taken from the Allen database<sup>22</sup>. The same values are used for all simulations.*

C <sub>m</sub> (pF)	E	PV	SST	VIP
L1				37.11
L2/3	123.41	70.95	82.34	41.23
L4	80.16	81.21	132.86	40.3
L5	149.43	70.9	52.32	59.29
L6	99.96	49.65	96.09	65.87

*Table 5: Leak conductance for each group of cells<sup>22</sup>.*

$gL$ (nS)	E	PV	SST	VIP
L1				4.07
L2/3	2.47	9.49	3.17	6.4
L4	5.16	9.19	7.96	1.87
L5	16.66	5.21	3.43	6.52
L6	5.88	6.86	2.99	6.09

*Table 6: Refractory period for each group of cells<sup>22</sup>.*

$\tau_{ref}$ (ms)	E	PV	SST	VIP
L1				3.5
L2/3	3	1.26	1.85	2.75
L4	4.4	1.5	2.2	2.4
L5	4.25	1.85	1.9	2.55
L6	3.3	1.65	2.1	2.85

*Table 7: Resting membrane potential for each group of cells<sup>22</sup>.*

$V_{rest}$ (mV)	E	PV	SST	VIP
L1				-65.5
L2/3	-80.97	-82.35	-69.16	-67.94
L4	-72.53	-70.45	-74.2	-63.14
L5	-68.28	-77.5	-70.01	-72.00
L6	-77.5	-76.42	-62.99	-78.85

*Table 8: Spike threshold for each group of cells<sup>22</sup>.*

$V_{th}$ (mV)	E	PV	SST	VIP
L1				-40.20
L2/3	-40.53	-56.32	-39.95	-41.34
L4	-47.63	-44.23	-44.07	-40.89
L5	-40.55	-51.2	-47.38	-51.2
L6	-42.31	-49.06	-37.19	-44.81

*Table 9: Background noise level that each group is receiving. Values represent the Poisson generator rates  $v_{bkgnd}$ .*

Rate of Poisson generator $v_{bkgnd}$ (Hz)	E	PV	SST	VIP
L1				650
L2/3	736	2949	631	1079
L4	1077	1894	2006	152
L5	3460	1399	648	1394
L6	1525	1540	590	1609